

**Molecular Genetic Studies on Secondary Cell Wall Deposition
during Xylem Vessel Cell Differentiation**

道管細胞分化過程における二次細胞壁蓄積メカニズムの
分子遺伝学的研究

1381006

Yuto Takenaka

Nara Institute of Science and Technology

Graduate School of Biological Science

Laboratory of Plant Metabolic Regulation

(Professor Taku Demura)

2016/03/15

Content

1. Introduction	3
1.1. What is secondary cell wall (SCW)?	3
1.2. Cellulose biosynthesis	4
1.3. Hemicellulose biosynthesis	6
1.4. Lignin biosynthesis	7
1.5. Deposition mechanisms of SCW biopolymers	8
1.6. Artificial induction system with transcriptional switches on xylem vessel cell formation	9
2. Materials and Methods	12
3. Results	16
3.1. Forward genetic screen for loss of SCW pattern identifies <i>baculites</i>	16
3.2. <i>baculites</i> shows <i>irregular xylem (irx)</i> mutant phenotypes	17
3.3. <i>CESA7</i> gene is responsible for the phenotype of <i>baculites</i>	18
3.4. Xylan deposition is prior to cellulose deposition during protoxylem vessel cell formation	19
3.5. Helical pattern of xylan deposition is dependent on cortical microtubules	20
3.6. Knock out mutant of <i>cesa7</i> shows abnormal, but patterned SCW deposition	21
3.7. Lacking of xylan biosynthesis does not affect cellulose deposition	22
4. Discussion	23
4.1. <i>baculites</i> is a novel allele of <i>irx</i> mutant with defects in <i>CESA7</i> function	23
4.2. Cellulose-independent xylan deposition during SCW formation	25
5. Table and Figures	28
6. Acknowledgements	45
7. References	46

1. Introduction

Xylem vessels make up the conductive system to transport water and minerals from roots to the whole plant body in vascular plants. The function of xylem vessels is indispensable for vascular plants, and can be one of limiting factors for plant growth and reproduction (Myburg et al., 2013). Thus, it is important to understand the molecular mechanisms of xylem vessel differentiation. The constituent cells of xylem vessels undergo secondary cell wall (SCW) formation and programmed cell death during cell differentiation. These cells have specific perforated ends to align end-to-end to form a continuous pipe structure to conduct water.

1.1. What is secondary cell wall (SCW)?

Cell walls are one of the characteristic structures of plant cells, and it is known that cell walls have critical roles, not only for cell morphology and intensity, but also for cell division and cell function in plants (Hamant and Traas, 2010; Wolf et al., 2012). Plant cells have two types of cell walls, primary cell wall (PCW) and SCW. Every plant cell has a PCW, which is the extensible wall synthesized during cell division and expansion. By contrast, SCW is a thick and rigid composite that is deposited only in certain types of cells, such as xylem vessels and fibers, following cell expansion. In these cells, SCW is produced between PCW and plasma membrane during their cell differentiation, and SCW is believed to impart mechanical stiffness and/or hydrophobicity to the xylem vessel cell, to serve as the conductive systems (Cosgrove and Jarvis, 2012). PCW and SCW are also distinguishable based on their composition; the typical PCW of dicot plants contains cellulose as main component, as well as xyloglucan as the major hemicellulose and gel-like pectin, whereas SCW is composed of a cellulose microfibrils embedded in a matrix of non-cellulosic polysaccharides, called xylan as the major hemicellulose in SCW, and phenolic compound lignin.

1.2. Cellulose biosynthesis

The most abundant component of SCW is cellulose, consisting of linear, unbranched β -1,4-glucans that are synthesized by the plasma membrane-localized huge complex called cellulose synthase complex (CSC) (reviewed in Bashline et al., 2014; McFarlane et al., 2014). The synthesized cellulose chains are crystalized into cellulose microfibrils and function as the main load-bearing polysaccharide. The CSC was firstly documented as the rosette structured complex by freeze fracture experiments and found to be localized at the end of microfibrils (Mueller et al., 1976). The identification of cellulose synthase at the molecular level was firstly achieved in the cellulose-producing bacteria *Acetobacter xylinum* (reviewed in Delmer, 1999). Based on sequence similarity to *Acetobacter xylinum* cellulose synthase, currently 10 homologous genes for cellulose synthase subunits, called *CESA*, have been identified in the model plant *Arabidopsis thaliana* (*Arabidopsis*) genome (Pear et al., 1996). The numbers of cellulose chain in one microfibril is estimated to be 12-36, therefore one CSC is thought to be composed of less than 36 *CESA* subunits (reviewed in Guerriero et al., 2010). PCW-type CSC is composed from subunits such as *CESA1*, *CESA3* and *CESA6* or other *CESA6*-like proteins. The SCW-type subunits were successfully identified through the molecular analysis of *irregular xylem (irx)* mutants (Turner and Somerville, 1997), in which xylem vessel cells are collapsed because of lack of enough cell wall strength of xylem tissues. It is widely accepted that in *Arabidopsis*, the three *IRX5/CESA4*, *IRX3/CESA7* and *IRX1/CESA8* proteins are essential for normal cellulose synthesis in SCW (Bashline et al., 2014; McFarlane et al., 2014). When one of subunits is lost, the remaining two subunits are not able to interact anymore (Taylor et al., 2003), all the three *CESA* proteins are found to be required to assemble functional SCW-specific CSC. However, several lines of experiments also suggested the overlapped functions of PCW-type *CESA* proteins and SCW-specific *CESA*; the SCW-specific *CESA7* can partially suppress the phenotypes of *cesa3*, in which the PCW-type *CESA3* protein was defective, and conversely, the PCW-type *CesA1* can partly rescue the phenotype of *irx1/cesa8* mutant (Carroll et al., 2012). Interestingly, the hybrid PCW-type CSC containing *CESA7* showed higher velocity than native PCW-type CSC (Carroll et al., 2012). Recently the visualization of SCW-specific *CESA7* protein during xylem vessel cell differentiation revealed that the velocity of SCW-type CSC movement is faster

than that of PCW-type CSC, possibly leading to efficient cellulose biosynthesis in SCW (Watanabe et al., 2015). These findings suggested the functional characteristics of CSC would largely depend on each CESA subunit protein, and the composition of subunits.

One of the critical factors for CSC function in cellulose biosynthesis at plasma membrane is the array of cortical microtubules (Gutierrez et al., 2009). In vascular plants, two types of xylem vessel cells, protoxylem-type and metaxylem-type vessel cells, are known to be differentiated depending on developmental stages (Schuetz et al., 2012); protoxylem- and metaxylem-type vessel cells have helical- and pitted-patterned SCW, respectively. Previous observations revealed that such patterned SCW deposition is dependent on the reorientation of cortical microtubules to helical- and pitted-alignment (Hepler and Newcomb, 1964). Molecular biological approaches successfully have made clear that the cortical microtubules can target CSC to the plasma membrane, and then guide the CSC movement during cellulose synthesis (reviewed in Crowell et al., 2010); disorganization of cortical microtubules by microtubule depolymerizing chemicals leads to decreased motility of CSC and malfunction in cellulose orientation (Baskin et al., 2004). For the physical interaction between CSC and microtubules, several interacting proteins have been identified. Cellulose Synthase Interacting Protein1 (CSI1) and its homologs are the associating proteins of all PCW-type CESAs and function as the linker between microtubule and CSC (Gu et al., 2010; Li et al., 2012; Bringmann et al., 2012). Knock-out mutation of *CSII* resulted in mis-colocalization of CSC and microtubules. Recently, the proteins named Companion of Cellulose synthase 1 (CC1) and CC2 were identified as proteins that interact with both PCW-type CSC and microtubules (Endler et al., 2015). Interestingly, CC1 and CC2 can promote CSC reassembly under salt stress conditions, thus they are hypothesized to be stress condition-specific regulators of the interaction between CSC and microtubules, to make robust synthesis of cellulose under adverse conditions (Endler et al., 2015). In the case of SCW formation during xylem vessel cell differentiation, xylem vessel cell-specific transmembrane proteins, Tracheary Element Differentiation-Related6 (TED6) and TED7 has been reported to function as the linker between CESA7 and cytoskeletal proteins (Endo et al., 2010; Rejab et al., 2015), These findings suggest the possibility that situation-specific linker proteins between CSC

and microtubules regulate cellulose synthesis by modulating the guidance of CSC along cortical microtubules.

Moreover, additional auxiliary proteins of CSC also seem to regulate cellulose deposition. KORRIGAN (KOR), a putative endo- β -1,4-glucanase, was shown to be a partner of PCW-type CSC, probably functioning to prevent aggregation of cellulose chains (Vain et al., 2014). However, compared to the case of PCW-type CSC, auxiliary proteins of SCW type-CSC are still not well understood.

1.3. Hemicellulose biosynthesis

Hemicellulose is non-cellulosic, heterogeneous polysaccharides which form networks via hydrogen-bonding with cellulose. Such features would contribute to produce the rigidity of SCW. Since hemicellulose contains many kinds of polysaccharides, its components and abundance vary according to species, cell types, developmental stages, and even in the positions within the wall of one cell (Pauly and Keegstra, 2010). In the case of SCW found in xylem tissues of dicot plants, xylan is the major hemicellulose consisting of a backbone of β -1,4-linked xylose units substituted with acetyl glucuronic acid, 4-*O*-methylglucuronic acid, and arabinose. The binding between cellulose microfibrils and xylans is considered to be critical for strength and elasticity of cell walls (reviewed in Faik, 2010).

Based on many observations, hemicellulosic components are thought to be synthesized in Golgi apparatus (Duplee and Sherrier, 1998), and then exported to the cell wall region by exocytosis (Northcote and Pickett-Heaps, 1966). Again, the *irx* mutants were one of important key materials to reveal hemicellulose biosynthetic genes (reviewed in Pauly et al., 2013). The current model suggested that putative glycosyltransferases IRX9, IRX10, and IRX14, and their closely related proteins IRX9L, IRX10L, and IRX14L, are involved in xylan backbone synthesis, and IRX7, IRX8, and PARVUS function in the synthesis of a primer or the reducing end for xylan (reviewed in Pauly et al., 2013). Other important enzymes participating in xylan biosynthesis are glucuronyltransferases, Glucuronic Acid Substitution1 (GUX1) and GUX2, which are required for the substitution of the xylan backbone with 4-*O*-methylglucuronic acid (Mortimer et al., 2010; Rennie et al., 2012). GUX1 and GUX2 have distinct preferences

to decorate xylan with 4-*O*-methylglucuronic acid (Bromely et al., 2013), and the fact that xylan without the 4-*O*-methylglucuronic acid substitution in *gux1 gux2* double mutant showed an increase in extractible xylan in mild alkali (Mortimer et al., 2010), suggests that xylan decoration with 4-*O*-methylglucuronic acid by GUX1 and GUX2 might be one of critical factors to determine the crosslinking ability of xylan to cellulose and/or lignin to affect the chemical and mechanical properties of SCW (Bromely et al., 2013).

1.4. Lignin biosynthesis

The other important component of SCW is lignin, the phenolic biopolymer that provides strong rigidity and hydrophobicity to cell walls (reviewed in Vanholme et al., 2010). Lignin is a complex polymer generated by oxidative combinatorial coupling of 4-hydroxyphenylpropanoids. The structure of lignin is complex and heterogenic due to its random radical coupling in the SCW matrix, and thus any fixed primary structure of lignin is not found. Recent NMR-based structural analysis revealed that lignin is likely associated with hemicellulosic carbohydrates through benzyl ether, γ -ester and phenyl glycoside linkages in SCW (Balakshin et al., 2011; Yuan et al., 2011).

The monomer units of lignin, called monolignols, are hydroxycinnamyl alcohols: typical types of lignin found in vascular plants is made from coniferyl alcohol, sinapyl alcohol, and *p*-coumaryl alcohol. These monolignols are speculated to be synthesized in the cytosol regions close to the endoplasmic reticulum, because it is shown that key enzymes of monolignol biosynthesis, such as cytochrome P450 enzymes Cinnamate 4-Hydroxylase, *p*-Coumarate 3-Hydroxylase, and Ferulate 5-Hydroxylase, are membrane proteins localized in the endoplasmic reticulum with the enzymatic active sites at the cytosolic side (Bonawitz and Chapple, 2010). The monolignol biosynthesis is started with phenylalanine, which is produced by the shikimate biosynthetic pathway in the plastid, through the phenylpropanoid pathway followed by the monolignol-specific metabolic pathways (Vanholme et al., 2010). The monolignols are transported from cytosol to the cell wall by certain molecular mechanisms; however, the details on monolignol transport have remained elusive. Although several reports suggested the involvement of ATP-binding cassette-like transporters in monolignol transport (Miao and Liu, 2010;

Arejandro et al., 2012) and proton-dependent transporters for monolignol glucosides (Tsuyama et al., 2013), it is still the matter under discussion.

The lignin units made from coniferyl alcohols, sinapyl alcohols, and *p*-coumaryl alcohols, are called guaiacyl (G), syringyl (S), and *p*-hydroxyphenyl (H) units, respectively. The molecular structure of each lignin units is different, and the composition of lignin units is different by plant species as well as by cell types, thus it is supposed that the composition of lignin units is a critical factor for SCW properties (Vanholme et al., 2010). Recently, monolignol polymerization in SCW of xylem tissues has been revealed to be executed by a set of laccases, oxidative enzymes. In the *Arabidopsis* triple mutants of *LACCASE4* (*LAC4*), *LAC11*, and *LAC17*, the lignin deposition of SCW was significantly decreased in the inflorescence stem (Berthet et al., 2011; Zhao et al., 2013). Moreover, Schuetz et al. (2014) demonstrated the high mobility of exported monolignols in cell wall as well as the targeted localization of *LAC4* and *LAC17* at specific SCW domains during protoxylem vessel cell differentiation, suggesting that the regulation of the polymerization step by laccases is a primary determinant of lignin patterning in SCW.

1.5. Deposition mechanisms of SCW biopolymers

Previous electron-microscopic and autoradiographic studies on the SCW polymers have suggested that cellulose is deposited at cell surface, and lignin is deposited within the preexisting wall structure (Ray, 1967; Hepler et al., 1970). The manner of hemicellulose deposition seems to be more complicated, the observations collectively suggest that the hemicellulose is produced by the Golgi and deposited by secretory vesicles over the course of SCW synthesis. (Northcote et al., 1989; Awano et al., 1998). In addition, lignin deposition is not observed without prior deposition of polysaccharides (Terashima et al., 1998). Taken into consideration the fact that the plasma membrane-localized CSC is responsible for cellulose synthesis and microtubule orientation is an critical determinant of CSC localization (Bashline et al., 2014; McFarlane et al. 2014) together, the currently-accepted view of SCW polymers can be summarized as 1) SCW formation is initiated with rearrangement of cortical microtubule network to delimitate areas of SCW formation, 2) cellulose synthases are secreted to the MT-enriched plasma membrane

domains and cellulose biosynthesis occurs at cell surface, 3) hemicellulose is simultaneously or subsequently deposited via secretory vesicles and may form hydrogen-bond with cellulose, and 4) monolignols are exported to the cell wall and polymerized into lignin by SCW-localized oxidative enzymes (Figure 1). However, there is still not enough experimental evidence to support this model being accurate to explain SCW deposition. Since native xylem vessels locate deep inside tissues and most of cells are dead, it is quite tough to get high-resolution images and track whole process of SCW deposition.

1.6. Artificial induction system with transcriptional switches of xylem vessel cell formation

Additional powerful tools to investigate SCW biosynthesis are artificial induction systems of xylem vessel cell formation using model plant systems such as *Zinnia elegans* and *Arabidopsis* (Fukuda and Komamine, 1980; Demura et al., 2002; Kubo et al., 2005; Pesquet et al., 2010). One of the striking achievements of the induction systems is the identification of transcriptional regulators of SCW biosynthesis; Kubo et al. (2005) successfully identified the plant-specific NAM, ATAF1,2, and CUC2 (NAC) transcription factors VASCULAR-RELATED NAC-DOMAIN (VND6) and VND7 as master regulators of differentiation of metaxylem and protoxylem vessel cells, respectively. After a lot of molecular (reverse) genetics research on VND and VND-related genes, the NAC protein subfamily Ic was identified by Zhu et al., (2012), containing VND and VND-related proteins such as SECONDARY WALL-ASSOCIATED NAC DOMAIN PROTEIN 1/NAC SECONDARY WALL THICKENING PROMOTING FACTOR3 and SOMBRERO, where were shown to possess the capacity to induce SCW biosynthesis (Mitsuda et al., 2005, 2007; Zhong et al., 2006, 2007; Willemsen et al., 2008; Benette et al., 2010). This family is conserved among a wide range of plant species, including non-vascular land plants taxa such as bryophytes (Zhu et al., 2012; Xu et al., 2014; Nakano et al., 2015).

The artificial induction system of VND6 or VND7 activity (Oda et al., 2010; Yamaguchi et al., 2008; Yamaguchi et al., 2010) further enhanced the research activity to reveal the detailed processes of SCW deposition. Transcriptome analysis using the

induction system showed the complexity of transcriptional regulatory network for SCW biosynthesis and a lot of key players of SCW biosynthetic enzymes (Zhong et al., 2010; Ohashi-Ito et al., 2010; Yamaguchi et al., 2011; Nakano et al., 2015). Also, the induction system greatly improved experimental accessibility to differentiating xylem vessel cells, which lie endogenously deep within plant tissues. As a result, fruitful cytological information about xylem vessel cell differentiation could be obtained, which includes 1) roles of microtubules-related proteins, MIDD1, Kinesin13A, and Rho GTPase Rop11 in the microtubule organization regulating metaxylem-type patterned SCW deposition (Oda et al., 2010; Oda and Fukuda, 2012, 2013), 2) control of lignin monomer cross-linking during protoxylem-type patterned SCW deposition (Schuetz et al., 2014), and 3) the higher velocity and density of SCW-specific CSC, compared to primary cell wall-specific CSC (Watanabe et al., 2015).

To obtain novel insights into the process of SCW deposition, here I used the transgenic *Arabidopsis VND7-VP16-GR* with the overexpression of *VND7* fused with the viral *VP16* transcription activation domain and the glucocorticoid receptor under the *35S* promoter, in which most of cells are subsequently transdifferentiated into protoxylem vessel cells in a synchronous manner by the application of glucocorticoid (Yamaguchi et al., 2011). Screening of ethyl methanesulfonate-mutagenized *VND7-VP16-GR* by microscopic observation successfully isolated the *baculites* mutant with flat cellulose deposition in ectopic protoxylem vessel cells. Several lines of evidence indicate that the responsible mutation for abnormality of *baculites* is located in the *CESA7* gene encoding a subunit of SCW-specific CSC. In *baculites*, C-terminal truncated *CESA7* protein would be produced because of the mutation. Of note, xylan and lignin deposition showed the clear helical patterns like normal SCW pattern of protoxylem vessel cells, while cellulose deposition was highly disordered in *baculites*. Detailed observation during xylem vessel cell differentiation demonstrated that xylan deposition is directed by the microtubule orientation, and it is prior to cellulose deposition. In addition, I found that the flat cellulose deposition was common among mutants with non-functional *CESA7* protein, but the knock-out *cesa7/irx3-4* and *cesa8/irx1-5* mutants deposited abnormal but patterned SCW whereas *cesa4/irx5-4* deposited relatively normal SCW. My results

suggest that SCW deposition will start with cellulose-independent xylan deposition during xylem vessel cell differentiation, and that the CesA4, 7 and 8 proteins have different contributions to SCW deposition.

2. Materials and Methods

Plant materials and plant growth condition

Arabidopsis (*Arabidopsis thaliana*) VASCULAR-RELATED NAC DOMAIN7 inducible line *VND7-VP16-GR* was described in Yamaguchi et al. (2010). The *Arabidopsis cesa7* mutants, *irx3-4* (Brown et al., 2005), *mur10-2* (Reiter et al., 1997; Bosca et al., 2006), *cesa8* mutant, *irx1-5* (Brown et al., 2005), and *cesa4* mutant, *irx5-4* (Brown et al., 2005) were kindly provided by the Arabidopsis Biological Research Center. Plants of *irx10/10l* in which *UBQ10pro::VND7-VP16-GR* was introduced were kindly provided from Dr. Mathias Schuetz of University of British Columbia, Vancouver, Canada. Arabidopsis seeds were sown on Murashige and Skoog (MS) medium containing 0.5% (w/v) sucrose solidified with 0.6% (w/v) gellan gum, and grown under continuous light condition at 22°C after a cold treatment at 4°C under dark condition for 1 to 2 days. For long-term growth of plants, 3-week-old plants grown on medium were transferred to soil and further grown at 22°C under long-day (16 h light/8 h dark) conditions.

DEX and oryzalin treatment

For the induction of the *VND7-VP16-GR* activity, 6-day-old seedlings grown on the medium were soaked in one-half-strength MS medium with 10 μ M DEX under continuous light condition at 22°C (Yamaguchi et al., 2010). The treated samples were sampled after 3 to 4 days of incubation in the DEX solution, or at the time points indicated in each experiment. When plants were treated with the microtubule polymerization inhibitor, oryzalin, 6-day-old seedlings grown on the medium were soaked in one-half-strength MS medium containing both 10 μ M DEX and 10 μ M oryzalin. To monitor the *Ubq10pro::GFP-TUB6* signals, the incubation with DEX and oryzalin were performed under dark condition at 22°C for 16 hours.

Histological observations

For the observations of SCW, samples were incubated in clearing solution (8:1:2 (w/v/v) mixture of chloral hydrate, glycerin, and water) for at least one night. Observations were made under a microscope equipped with Nomarski optics and a digital camera system (BX53-DIC and DP72; Olympus).

For sectioning, 6-day-old wild-type seedlings were fixed in FAA solution (3.7% (v/v) formaldehyde, 50% (v/v) ethanol, 5% (v/v) acetic acid) for 1 h, and dehydrated with ethanol series of 50%, 60%, 70%, 80%, 90%, 100% for 30 min at room temperature. Then, the samples were incubated in 100% ethanol for one night at 4°C. The dehydrated samples were embedded in Technovit 7100, according to manufacturer's protocols (Heraeus-Kulzer). 6 μ m-Sections were made by a microtome (PR-50, YAMATO KOHKI), followed by the staining with toluidine blue-O.

EMS mutagenesis and mutant screening

Seeds of *VND7-VP16-GR* were incubated with 0.3% (v/v) ethyl methanesulfonate (EMS; Sigma) solution for 8 h incubation with gentle shaking at room temperature to obtain M1 seeds. After the EMS treatment, M1 seeds were repeatedly washed with 80-ml distilled water 12 times (30-sec incubation \times 5, 30-min incubation \times 2, and then 30-sec \times 5). Washed M1 seeds were sown on MS medium, and grown for 3 weeks. M1 plants were separately transferred into soil for further growing, and then M2 seeds were harvested after the self-reproduction of each M1 plant independently. The M2 lines were subjected to the DEX treatment, and observed to isolate mutants with abnormal SCW formation.

Cell wall labeling

Cellulose staining was performed with 10 mg/ml pontamine S4B (Sigma) in one-half-strength MS medium for 10 min and washed twice in one-half-strength MS medium. For xylan immunostaining, seedlings were fixed with FAA for 1 h, and washed with 50% and 20% ethanol for 10 min and stored in TBST solution (10 mM Tris-HCl (pH 7.0), 0.25 M NaCl, 0.1 % (w/v) Tween 20). Samples were then incubated in 5 % (w/v) bovine serum albumin in TBST for 1 h at room temperature, followed anti-xylan antibody LM10 (plant probes; McCartney et al., 2005) at 1:36 dilution overnight at 4 °C. Samples were washed

with TBST three times, and incubated with goat anti-rat IgG CFL-488 (Santa Cruz) or Alexa-488 (Invitrogen) at 1:100 dilution at room temperature for 3 h with gentle shake. After washing three times with TBST, samples were mounted in one-half-strength MS medium after pontamine S4B staining and observed. Observations of cell wall labels were made by deconvolution microscope (DeltaVision Elite, GE Healthcare) equipped with photometrics cool snap HQ2 camera, and/or Perkin-Elmer UltraView Vox spinning disk confocal mounted on a Leica DMI6000 inverted microscope equipped with Hamamatsu 9100-02 CCD camera. Excitation and emission filters were set to FITC (475 and 525) and TRITC (542 and 593) or GFP (488 and 525) and RFP (561 and 595). Lignin autofluorescence was observed using a FV1000 Multiphoton Laser Scanning Microscope (Olympus) with a tunable MaiTai BB DeepSee laser adjusted to 730nm.

Quantitative RT-PCR

Total RNA was extracted using RNeasy Plant Mini Kit (Qiagen), and then treated with RQ1 RNase-Free DNase (Promega). 1 μ g of DNase-treated total RNA was reverse-transcribed by Transcriptor Reverse transcriptase (Roche) with oligo (dT) 18 primer. Quantitative PCR from this cDNA was performed with the SCW-related gene-specific primers (described in Yamaguchi et al., 2010) using LightCycler[®] 480 system (Roche) according to the manufacturer's protocols. *UBQ10* was used as an internal control.

Monosaccharide analysis

Seedlings of *VP16-GR*, *VND7-VP16-GR*, in wild-type and *baculites* backgrounds, were incubated with or without 10 μ M DEX for 5 days. Samples were dried at 45[°] C overnight and subsequently ground in a Wiley mill to pass a 40 mesh screen and treated with acetone overnight using a Soxhlet and then dried for 48 h at 50[°] C. Approximately 10 mg (4 replicates per sample) of dried extractive-free tissue was treated with 72% sulphuric acid for 2 h, diluted to ~3% with 112-ml distilled water and autoclaved at 121[°] C for 60 min. The mixture was filtered through a medium coarseness crucible and the carbohydrate content of the filtrate was determined by HPLC analysis. Glucose, xylose, mannose, galactose, arabinose and rhamnose were analyzed using a Dx-600 anion-exchange HPLC (Dionex) with a CarboPac PA1 column (Dionex) at 1 ml/min and post

column detection (100mM NaOH/min). Sugar concentrations were calculated from standard curves created from external standards. This experiment was performed by Dr. Faride Unda and Prof. Shawn D Mansfield in University of British Columbia, Vancouver, Canada.

Plant transformation

The *CESA7pro::YFP-CESA7* and *Ubq10pro::GFP-TUB6* plasmids were kindly provided by Mr. Yoichiro Watanabe (University of British Columbia, Vancouver, Canada) and Dr. Takashi Hashimoto (NAIST, Japan; Nakamura et al., 2004), respectively. The plasmids were electroporated into *Agrobacterium tumefaciens* strain GV3101/pMP90. A simplified version of the floral dip method was used for plant transformation (Clough and Bent, 1998).

3. Results

3.1. Forward genetic screen for loss of SCW pattern identifies *baculites*

The *35S::VND7-VP16-GR* (wild-type *VND7-VP16-GR*) seeds (Yamaguchi et al., 2010) were mutagenized by ethylmethanesulfonate to obtain M1 plants, which were subsequently individually grown to harvest the independent M2 seeds (Figure 2). To isolate mutants with defective SCW deposition, I performed microscopic observation of SCW formed in transdifferentiated epidermal cells from M2 seedlings treated with 10 μ M dexamethasone (DEX) for 3 days (Figure 2). By the screening of more than 2000 lines, I successfully isolated the recessive mutant line called *baculites VND7-VP16-GR* (Figure 3), named for a smooth ammonite which lacked the helical characteristics of these extinct molluscs. While the parental *VND7-VP16-GR* differentiated ectopic vessel cells with the clear helical SCW characteristics of protoxylem vessel cells, plant lines expressing *VND7-VP16-GR* in *baculites* background (*baculites VND7-VP16-GR*) did not show the helical patterned SCW of ectopic xylem vessels (Figure 3A-D). Monosaccharide analysis on the DEX-treated seedlings showed that induction of protoxylem vessel cell differentiation resulted in large, nearly identical increase in glucose and xylose in both wild-type *VND7-VP16-GR* and *baculites VND7-VP16-GR* (Table 1). The data is consistent with previous observation on cell wall fractions of *VND7-VP16-GR* which showed increased glucose and xylose accumulation during xylem vessel cell differentiation induced by the DEX treatment (Table 1; Yamaguchi et al., 2010), indicating that in *baculites VND7-VP16-GR*, SCW formation can be initiated, but its deposition pattern is abnormal.

For the detailed phenotypic analysis, I next visualized the cell wall components of ectopic SCW in wild-type *VND7-VP16-GR* (Figure 4A-C) and *baculites VND7-VP16-GR* (Figure 4D-F). Cellulose was visualized histochemically with pontamine fast scarlet 4B, which is a cellulose-specific fluorescence stain (Anderson et al., 2010), while xylan was visualized by immunostaining using the anti-xylan antibody LM10 (McCartney et al., 2005), and then observed by confocal laser scanning microscope. The signal of cellulose and xylan colocalized at the SCW domain in wild-type *VND7-VP16-GR* (Figure 3A-C). In contrast, *baculites VND7-VP16-GR* lacked the patterned cellulose signals, and instead

a uniform deposition of cellulose was observed (Figure 4E). Notably, I found that the pattern of xylan deposition was unaffected but patchy in *baculites VND7-VP16-GR* (Figure 4D). Line scans of the cellulose stain and anti-xylan signal, which were sampled along the long axis of the same induced protoxylem cell, showed tight correlation of the two wall components in wild-type *VND7-VP16-GR* (Figure 4G), while in *baculites VND7-VP16-GR*, the cellulose signal was uniform but the xylan signal showed clearly defined peaks (Figure 4H).

In order to evaluate if lignin deposition was also altered in *baculites VND7-VP16-GR*, I employed multiphoton UV-excitation microscopy to document lignin autofluorescence. A helical pattern of lignin was observed in induced protoxylem cells in both wild-type *VND7-VP16-GR* (Figure 5A) and *baculites VND7-VP16-GR* (Figure 5B), indicating that patterned deposition of lignin is unaffected in *baculites VND7-VP16-GR*. Contrasting the line scans from wild-type *VND7-VP16-GR* cells (Figure 4G) and *baculites VND7-VP16-GR* cells (Figure 4H), I found both showed regular peaks (Figure 5B, D), unlike cellulose signal (Figure 4H). These findings indicate that *baculites VND7-VP16-GR* is a unique mutant that shows uncoupled deposition of cellulose from other SCW components such as xylan and lignin.

3.2. *baculites* shows irregular xylem (*irx*) mutant phenotypes

I checked if *baculites VND7-VP16-GR* plants had defects in formation of endogenous xylem vessel cells in the roots. Histological observations indicated that, compared with root from wild-type *VP16-GR* (Figure 6A) or roots from wild-type *VND7-VP16-GR* (Figure 6B, un-induced), the xylem vessels of *baculites VND7-VP16-GR* were irregularly shaped and frequently collapsed (Figure 6C, un-induced). Furthermore, two-month-old plants of *baculites VND7-VP16-GR* showed severely dwarfed phenotypes, and the inflorescence stem did not stand straight (Figure 6D). These all phenotypes are commonly found in *irregular xylem (irx)* mutants, which show collapsed xylem vessel cells and decreased mechanical strength in inflorescence stem (Turner and Somerville, 1997; Taylor et al., 1999; Brown et al., 2005). Thus, I concluded that *baculites* can be categorized as a new *irx* mutant.

To further examine the abnormalities of SCW formation in *baculites VND7-VP16-GR*, I performed quantitative RT-PCR analysis on SCW-related genes, including genes integral to cellulose biosynthesis (*CESA4/IRX5*, *CESA7/IRX3*, and *CESA8/IRX1*; Pear et al., 1996; Turner and Somerville, 1997; Taylor et al., 1999), hemicellulose biosynthesis (*IRX8* and *IRX10*; Brown et al., 2005), and lignin biosynthesis (*LAC4/IRX12*; Brown et al., 2005) using total RNA extracted from 6-day-old seedlings grown with or without DEX. In wild-type *VND7-VP16-GR* plant lines, all the genes examined were upregulated by the DEX treatment, as previously reported (Figure 3A; Yamaguchi et al., 2010). Among the tested genes, only *CESA7* expression was significantly decreased in *baculites VND7-VP16-GR* (Figure 7). When ectopic protoxylem was induced in *baculites VND7-VP16-GR*, *CESA7* expression did increase, but the transcript abundance was significantly lower compared to wild-type *VND7-VP16-GR* (Figure 7). This implies the hypothesis that the abnormal cellulose deposition apparent in *baculites VND7-VP16-GR* could be attributed to a problem with the expression of *CESA7*.

3.3. *CESA7* gene is responsible for the phenotype of *baculites*

Taking the results described above, I sequenced the genomic region of *CESA7* gene, and found a single nucleic acid substitution (G to A transition) at the splice acceptor site of the 8th intron (Figure 8A). RT-PCR analysis followed by sequencing analysis on the *CESA7* cDNA revealed that the G to A substitution in *baculites VND7-VP16-GR* caused the change in the splice acceptor site to the following AG site, 13 bp downstream. The altered splicing is predicted to result in a frame shift to generate an isoleucine to valine substitution, followed by a premature stop codon at position 578 (Figure 8B). Introduction of *CESA7pro::YFP-CESA7* into *baculites VND7-VP16-GR* showed recovery from all defects, including irregularly shaped and collapsed xylem vessel cells (Figure 9A-C) and growth phenotype (Figure 9D). In addition, the helical patterned SCW was clearly observed in the ectopic xylem vessel cells induced after DEX treatment in *baculites VND7-VP16-GR* carrying *CESA7pro::YFP-CESA7* (Figure 9E-G). These results indicate that the phenotypes of *baculites VND7-VP16-GR* can be attributed to a mutation in *CESA7* gene. The mutation in *baculites VND7-VP16-GR* caused a frame shift and the premature stop codon because of change in splicing site at the 8th intron (Figure

8B). As a result, it was expected that the the mutation in *baculites VND7-VP16-GR* manifested in a 578 N-terminal amino acids CESA7 protein consisting of an additional Val residue, which corresponds to the N-terminal region, two transmembrane domains, and a truncated central cytoplasmic region (Figure 10). Thus, the mutated CESA7 protein in *baculites VND7-VP16-GR* lacks the C-terminal region containing the latter catalytic domain and 6 transmembrane domains, suggesting the CESA7 protein in *baculites VND7-VP16-GR* is a non-functional form.

3.4. Xylan deposition is prior to cellulose deposition during protoxylem vessel cell formation

In *baculites VND7-VP16-GR*, despite the uniform cellulose deposition, the weak xylan signals were detected in the helical patterns typical of protoxylem cells (Figure 4D). To further define the timing of cellulose and xylan deposition, I performed time-sequential observations of induced wild-type *VND7-VP16-GR* and *baculites VND7-VP16-GR*. Six-day-old seedlings of both lines were treated with DEX, and then subjected to fixation over a defined time course (0 to 6 hours, 6 to 7.5 hours, 7.5 to 15 hours, and after 15 hours of DEX treatment, respectively) of SCW deposition (Figure 11). In both of wild-type and *baculites VND7-VP16-GR*, the first indication of SCW deposition was derived from xylan signals, which were apparent between 6 to 7.5 hours after DEX treatment (Figure 11D, L, R, V). The xylan signals were patchy, but were aligned in a helical pattern. At this stage, no obvious cellulose signal was detected using pontamine S4B, indicating that xylan deposition could precede cellulose deposition. Following 7.5 to 15 hours after DEX treatment, the helical signals of cellulose appeared and colocalized with xylan in wild-type *VND7-VP16-GR* (Figure 11E-F, S) and was really obvious after 15 hours (Figure 11G-H, T). In contrast, *baculites VND7-VP16-GR* did not exhibit any patterned cellulose signal following the DEX treatment (Figure 11I, K, M, O). However, after 7.5 hours of DEX treatment, the intensity of uniform cellulose signals appeared to become stronger gradually, but no pattern was detected (Figure 11M, O, W, X). It is noteworthy that the xylan signals of *baculites VND7-VP16-GR* were continuously patchy, and they did not become linear as observed in the wild-type *VND7-VP16-GR* (Figure 11H). These results suggested that while early xylan secretion into the SCW domain is

not influenced by cellulose deposition, the arrangement of xylan deposition within the SCW domains relies on the presence of cellulose.

3.5. Helical pattern of xylan deposition is dependent on cortical microtubules

Previous studies have shown that SCW formation is initiated with the rearrangement of cortical microtubule arrays, which play critical roles in determining the SCW patterning (Oda et al., 2005). In an attempt to resolve the mechanism of cellulose-independent xylan accumulation, I visualized cortical microtubules using the reporter *Ubq10pro::GFP-TUB6* (Nakamura et al., 2004). Six-day-old seedlings of wild-type and *baculites*, both which carried the *VND7-VP16-GR* and *Ubq10pro::GFP-TUB6*, were treated with DEX, for 16 hour under dark conditions, and subjected to microscopic analysis. In induced wild-type *VND7-VP16-GR* lines, the *Ubq10pro::GFP-TUB6* signals showed clear helical patterns with only DEX treatment (Figure 12A), and such patterns were disturbed by the addition of microtubule-depolymerizing drug oryzalin (Figure 12B). The GFP-TUB6 signals in *baculites VND7-VP16-GR* showed strong banding (Figure 12C), indicating that the microtubule rearrangement is normal during protoxylem vessel cell differentiation in *baculites*. This microtubule array was also disrupted by oryzalin in *baculites VND7-VP16-GR* (Figure 12D).

I next tested if the deposition patterns of cellulose and xylan in *baculites VND7-VP16-GR* were sensitive to microtubule depolymerization using oryzalin. The helical patterned deposition of cellulose and xylan was disrupted by the oryzalin treatment in wild-type *VND7-VP16-GR*, however, within the disorganized pattern, the co-localization of cellulose and xylan was maintained (Figure 13A-F). In *baculites VND7-VP16-GR*, the cellulose signals did not show any pattern, regardless the oryzalin treatment (Figure 13G, J). The helical xylan deposition (Figure 13H) was disordered by the oryzalin treatment (Figure 13K), and the wavy xylan patterns were similar to the disordered cortical microtubule arrays after the oryzalin treatment (Figure 12D). These observations indicated that the cellulose-independent xylan deposition is directed by the cortical microtubules at the early stage of SCW formation during protoxylem vessel cell differentiation.

3.6. Knock-out mutant of *cesa7* showed abnormal, but patterned SCW deposition

The induction system of xylem vessel cell differentiation, combined with the *baculites* mutant allele, revealed that secondary cell wall cellulose deposition can be uncoupled from the normal deposition of other secondary cell wall components. This approach has not been exploited for other mutant alleles of *CESA7*, and other SCW-specific *CESA* alleles. Therefore, I asked the question, is the uncoupled cellulose phenotype found in other alleles of *cesa*? I examined the mutants of *irx3-4/cesa7* (T-DNA insertion knock-out mutant) (Brown et al., 2005), *mur10-2/cesa7* allele (H-734-Y, Figure 10) (Bosca et al., 2006), *irx1-5/cesa8* (T-DNA insertion knock-out mutant) (Brown et al., 2005) and *irx5-4/cesa4* (T-DNA insertion knock-out mutant) (Brown et al., 2005) by crossing *VND7-VP16-GR* with each mutant to obtain *VND7-VP16-GR* homozygous for each mutation. With DIC, observations of SCW deposition in ectopic xylem vessel cells showed that, compared to the patterned wild-type *VND7-VP16-GR* (Figure 14A-B), effects of the *mur10-2* mutation are the loss of the SCW helical-pattern phenotype similar to that of *baculites VND7-VP16-GR* (Figure 14F-G). However, interestingly, the knock-out *irx3-4* mutant displayed abnormal, but patterned SCW thickening (Figure 14K-L). Specifically examining the cellulose with pontamine S4B, *mur10-2* lines resembled *baculites*, i.e. it was not arranged in the helical wall pattern as in *VND7-VP16-GR* (Figure 14D) but instead was uniform across the cell surface (Figure 14I). In the knock-out *irx3-4*, the pontamine S4B-stained cellulose was observed in a weak, but banded, distribution (Figure 14N). The xylan deposition pattern in both *mur10-2* and *irx3-4* mutants was within the helical SCW pattern (Figure 14H, M), although it was less well organized than wild-type *VND7-VP16-GR* (Figure 14C). The xylan signals in *irx3-4* were uneven (Figure 14M), and the margin of the secondary cell wall thickening was not smooth but undulating (Figure 14K-L). The contrast between the *cesa7* mutant phenotypes indicates that complete loss of the *CESA7* protein from the cellulose synthase complex in the knockout allele (*irx3-4*) produces a residual helical pattern of cellulose with a loosely associated secondary cell wall matrix, while the existence of a mutant or truncate *CESA7* protein in *mur10-2* or *baculites* led to a spatial uncoupling of cellulose deposition although the helical pattern of the SCW matrix persists.

My data also showed that mutations in the other components of the SCW CSC, such as *irx1-5/cesa8* (Figure 14P-T) exhibited similar SCW to *irx3-4* (Figure 14K-O). In contrast the SCW in *irx5-4/cesa4* (Figure 14U-Y) was similar to the wild type *VND7-VP16-GR* (Figure 14A-E). The helical deposition of cellulose found in these knock-out mutation of *CESA4*, 7 and 8, suggests that the cellulose synthase complex might be able to follow the guidance of microtubules, but the normal assembly of the SCW was impaired somewhat in the case of *irx1-5* and *irx3-4*. These findings might imply the different contribution of each CESA subunit in CSC for cellulose biosynthesis during SCW formation.

3.7. Lacking of xylan biosynthesis does not affect cellulose deposition

Finally, I evaluated cellulose deposition in xylan-deficient mutants during xylem vessel cell differentiation. I introduced the construct of *UBQ10pro::VND7-VP16-GR* into the double mutant of *irx10 irx10l*, in which no detectable LM10 signal was found in stem tissues because of the deficiency of xylan biosynthesis (Wu et al., 2009), and then I induced ectopic xylem vessel cell differentiation. Unlike strong xylan signal of the wild-type *VND7-VP16-GR* plants (Figure 15A), *irx10 irx10l VND7-VP16-GR* did not show any detectable LM10 signal (Figure 15C), as previously reported (Wu et al., 2009). However, the clear patterned cellulose signals could be observed in both the wild type *VND7-VP16-GR* and *irx10 irx10l VND7-VP16-GR* (Figure 15B, D). This result also supported the uncoupling between cellulose and xylan deposition, and can suggest that early-deposited xylan does not contribute to the patterning of cellulose deposition during SCW formation in protoxylem vessel cell differentiation.

4. Discussion

4.1. *baculites* is a novel allele of *irx* mutant with defects in *CESA7* function

In this study, I isolated *baculites* as a mutant showing SCW formation without the patterned deposition of cellulose, by the genetic screening of *VND7-VP16-GR* lines, in which ectopic protoxylem vessel cells can be induced (Figure 2). *baculites VND7-VP16-GR* showed the *irx* phenotype, *i.e.* collapsed xylems and stunted growth, and the single nucleic acid substitution in the 8th splicing acceptor site of *CESA7* was found in the genome of *baculites VND7-VP16-GR*, resulted in the decrease of *CESA7* mRNA level and C-terminal truncated protein product (Figure 7, 9). The increase in glucose and xylose monomers in the *baculites VND7-VP16-GR* was similar to those observed for wild-type *VND7-VP16-GR* (Table 1), suggesting that SCW biosynthesis occurred in *baculites* by the activation of VND7 activity. Monosaccharide analysis also showed that significant increase of arabinose in *baculites VND7-VP16-GR* regardless the DEX treatment (Table 1), consistent with the reports on different alleles of *cesa7* mutants, such as *fra5* and *mur10* (Zhong et al., 2003; Reiter et al., 1997). The introduction of *CESA7pro::YFP-CESA7* rescued the phenotype of *baculites VND7-VP16-GR* (Figure 8), indicating that *baculites VND7-VP16-GR* is a novel allele of *CESA7* mutants.

The view that *CESA7* is one of essential components of CSC for lignified SCW, and that the *CESA7*-containing CSC is guided by microtubules for the patterned SCW formation, are widely accepted (Bashline et al., 2014; Li et al., 2015; McFarlane et al., 2014; Wightman and Turner, 2008). In *baculites VND7-VP16-GR*, the amounts of glucose and xylose and cellulose signal intensities were increased after the DEX treatment as shown in wild-type *VND7-VP16-GR* (Table 1), suggesting that SCW biosynthesis occurred even in *baculites VND7-VP16-GR* by the activation of VND7 activity. My observations revealed that cellulose was deposited without any patterns in ectopic xylem vessel cells of *baculites VND7-VP16-GR*; cellulose accumulation was flat to cover whole cell surface in *baculites VND7-VP16-GR* (Figure 3), although cortical microtubules showed the helical arrangement (Figure 12). These results indicated disconnection between microtubules and CSC in *baculites*. The *mur10-2* mutation, which causes a point mutation at the cytosolic catalytic domain (H734Y) (Bosca et al., 2006),

resulted in similar phenotype to *baculites* (Figure 14). Interestingly, while the knock out mutant *irx3-4* showed abnormal SCW in ectopic xylem vessel cells, these SCW still formed the helical pattern (Figure 14). These suggested that the CSC containing non-functional CESA7 would have a problem with interaction with microtubules. It is also interesting to note that the lesions in both *mur10-2* or *baculites* mutants are in the cytosolic domain of CESA7 where interactions with accessory proteins are predicted to occur (Gu et al., 2010; Endler et al., 2015; Vandivasi et al., 2016)

Recently, a couple of proteins have been reported to function in the physical linkage between PCW-type CSC and microtubules (Gu et al., 2010; Bringmann et al., 2012; Li et al., 2012; Endler et al., 2015). Cellulose synthase interacting1 (CSI1), also known as POM2, was the first protein reported to bind to both CSC and microtubules, and is considered to be a key scaffold protein to guide CSC along cortical microtubules (Gu et al., 2010; Bringmann et al., 2012; Li et al., 2012). Additionally, companion of cellulose synthase (CC) was identified as an important regulator for microtubule assembly and CSC guidance under salt stress conditions (Endler et al., 2015). CC has binding activity to both CSC and microtubules, in addition to a transmembrane domain, suggesting that CC functions in the establishment of stable interaction between CSC and cortical microtubules at the plasma membrane. Previous data only showed that CSI1/POM2 and CC physically interact with PCW-type CesAs (Gu et al., 2010; Endler et al., 2015), but experiments in the *in vitro* Arabidopsis xylem vessel cell differentiation system suggested the involvement of CSI1/POM2 in SCW formation (Derbyshire et al., 2015). Moreover, previously the xylem vessel cell-specific transmembrane protein, Tracheary Element Differentiation-Related6 (TED6), which is important for SCW formation, was reported to interact with CESA7 (Endo et al., 2009; Rejab et al., 2015). These studies suggest a possible mechanism to explain the *baculites* phenotype: CSC containing non-functional CESA7 cannot interact with such proteins to form stable CSC-microtubule structure at the plasma membrane underlying the SCW. Without the ability to interact with microtubules, one can envision that mutated or truncated CESA7-containing CSC complexes could migrate away from the sites of secretion and track randomly along the plasma membrane. Indeed, visualizing the movement of CESA7-containing CSC during SCW formation using fluorescent protein-tagged CESA7 in *VND7-VPI6-GR* system

revealed that CSC are specifically localized to microtubule lined plasma membrane domains (Watanabe et al., 2015). My observations on knock-out mutants of *irx1-5/cesa8* and *irx5-4/cesa4* suggested the different contribution of each CESA protein in patterned cellulose deposition during SCW formation (Figure 14). Future analysis with similar fluorescent protein-tagged CSC in mutant background will provide clues as to function of CESAs..

4.2. Cellulose-independent xylan deposition during SCW formation

Immunolabelling observations revealed that weak, patchy but helical xylan deposition started before cellulose during xylem vessel cell formation (Figure 11). Similar early deposition of hemicellulosic polymers were observed in the *Zinnia* system by Hogetsu (1990) and in the metaxylem vessel cell differentiation system by Oda et al. (2005). Since the pattern of cortical microtubules is unaffected in *baculites VND7-VP16-GR*, the secretion of CSCs, xylan, and enzymes required for lignification such as laccases still occurs at these microtubule-enriched plasma membrane domains. Treatment with a microtubule-depolymerizing drug disturbed the helical deposition of xylan (Figure 13), indicating the early xylan deposition is directed by the helically-arranged cortical microtubules. This association between xylan and microtubules is consistent with previous observations (Zhu et al., 2015). Importantly, this early xylan deposition was also found in *baculites* and *mur10-2*, which are defective in CESA7 (Figure 14; Bosca et al., 2006), therefore, the early xylan deposition appears to be uncoupled with the regulation of cellulose deposition at SCW domain. I also found that the signals of xylan deposition became stronger and linear at SCW domains, after the cellulose deposition started (Figure 11). Such patterns in xylan signals were not detected in *baculites* and *mur10-2*, *i.e.* the xylan signals of *baculites* and *mur10-2* were not changed during SCW deposition (Figure 11). Therefore the deposited crystalized cellulose will affect the later xylan deposition. Currently, Busse-Wicher et al. (2014) proposed a model of interaction between cellulose microfibrils and xylan chains based on the observations of *Arabidopsis* using mass spectrometry and NMR, in which xylan would align with vacancies on cellulose microfibril hydrophilic surfaces. My observations of linear xylan deposition along cellulose signals might reflect such structural interaction. Taken these information

together, I propose new model that SCW deposition starts with xylan deposition followed by the cellulose, then, further hemicellulose and lignin associate with pre-existing wall polymer to form rigid SCW in protoxylem vessel cells of Arabidopsis (Figure 16).

What are the roles of cellulose-independent xylan deposition in SCW formation of xylem vessel cells? Although functions of xylan in SCW deposition are still elusive, *irx* mutants with defects in xylan biosynthesis clearly demonstrated the importance of xylan in SCW integrity (Zhong et al., 2005; Persson et al., 2007; Lee et al., 2007; Brown et al., 2008; Wu et al., 2010; Jensen et al., 2011; Brown et al., 2011). I revealed that the *irx10 irx10l* double mutations do not affect the patterned cellulose deposition (Figure 15), suggesting that the cellulose-independent xylan deposition has little contribution to the interaction between CSC and microtubules. The works using *in vitro* cellulose biosynthesis system with *Acetobacter xylinum* showed the addition of xylan greatly changed the cellulose features, probably through the influences on the cellulose aggregation (Atalla et al., 1993). In addition, the suppression of xylan endotransglycosylase activity was reported to affect angles of cellulose microfibrils in poplar (Derba-Maceluch et al., 2014), suggesting that xylan is one of determinants of cellulose features during SCW formation. Thus, pre-deposition of xylan might function as enhancer and/or moderator of the formation of SCW-type cellulose microfibrils, i.e. highly crystallized and polymerized cellulose. Or, it can be explained from the viewpoints of an interaction between other cell wall components, such as lignin and proteins. Utracki (2002) proposed the possibility that xylan acts as a compatibilizer between cellulose and lignin, by decreasing the interfacial tension between these two components. Reis and Vian (2004) also suggested that glucuronoxylan could provide lignin binding sites, via the glucuronic acid decorating xylan in an outwards fashion to coat cellulose microfibrils. It has already been demonstrated that laccase, a lignin polymerization enzyme, is delivered to the SCW domain directly at early stages of xylem vessel cell formation (Schuetz et al., 2014). It is not well understood how such cell wall enzyme proteins are delivered and anchored to specific regions of cell surface, but the lignin signals of *baculites VND7-VP16-GR* (Figure 5) suggested that the early deposition of xylan can provide sufficient binding sites to lignin as well as sufficient laccase activity. Taken all the information together, I suppose that the early deposition of xylan

may change the cell surface atmosphere chemically, possibly partly through chemically-different substituents of xylan as suggested in Busse-Wicher et al. (2014), to make a scaffold of SCW domain to solidify the cell wall structure. This scaffold may have a positive effect in anchoring proteins for lignification as well. This view does not conflict with recent observations of normal and compression wood of pine, in which changes in amount and localization of noncellulosic polysaccharides would mediate woody cell wall assembly (Donaldson and Knox, 2012). Further examination of SCW deposition and properties in my mutant as well as the other types of *irx* mutants including hemicellulose-deficient mutants is needed to verify that xylan deposition prior to cellulose deposition for the structural organization of SCW.

5. Table and Figures

	Hydrolized Sugars per cell wall material (ug/mg)					
	Ara	Rha	Gal	Glu	Xyl	Man
<i>VP16-GR</i>	18.0 ± 3.6	18.8 ± 1.7	45.4 ± 3.0	99.5 ± 4.6	14.3 ± 1.3	7.1 ± 0.3
<i>VP16-GR+DEX</i>	21.3 ± 1.6	18.7 ± 0.5	49.1 ± 1.2	105.8 ± 3.1	15.4 ± 0.6	7.4 ± 0.3
<i>VND7-VP16-GR</i>	15.7 ± 1.0	18.9 ± 1.0	45.4 ± 1.6	92.3 ± 4.3	13.6 ± 0.7	6.6 ± 0.3
<i>VND7-VP16-GR+DEX</i>	18.3 ± 0.7	17.3 ± 0.5	42.9 ± 1.5	139.9 ± 6.2	49.2 ± 2.2	6.5 ± 0.3
<i>baculites</i>	23.8 ± 1.3	14.8 ± 0.6	45.2 ± 2.6	98.4 ± 5.1	17.2 ± 0.8	8.0 ± 0.4
<i>baculites+DEX</i>	24.8 ± 0.4	20.0 ± 0.6	43.7 ± 1.0	169.4 ± 3.1	51.3 ± 0.7	9.4 ± 0.2

Table1. Monosaccharide analysis from whole seedlings

Monosaccharide composition of cell walls from seedlings of wild-type *VP16-GR*, wild-type *VND7-VP16-GR* and *baculites VND7-VP16-GR* with or without DEX treatment were determined by HPLC. Results are means ± SD (n=4). Ara, arabinose; Rha, rhamnose; Gal, galactose; Glu, glucose; Xyl, xylose; Man, mannose.

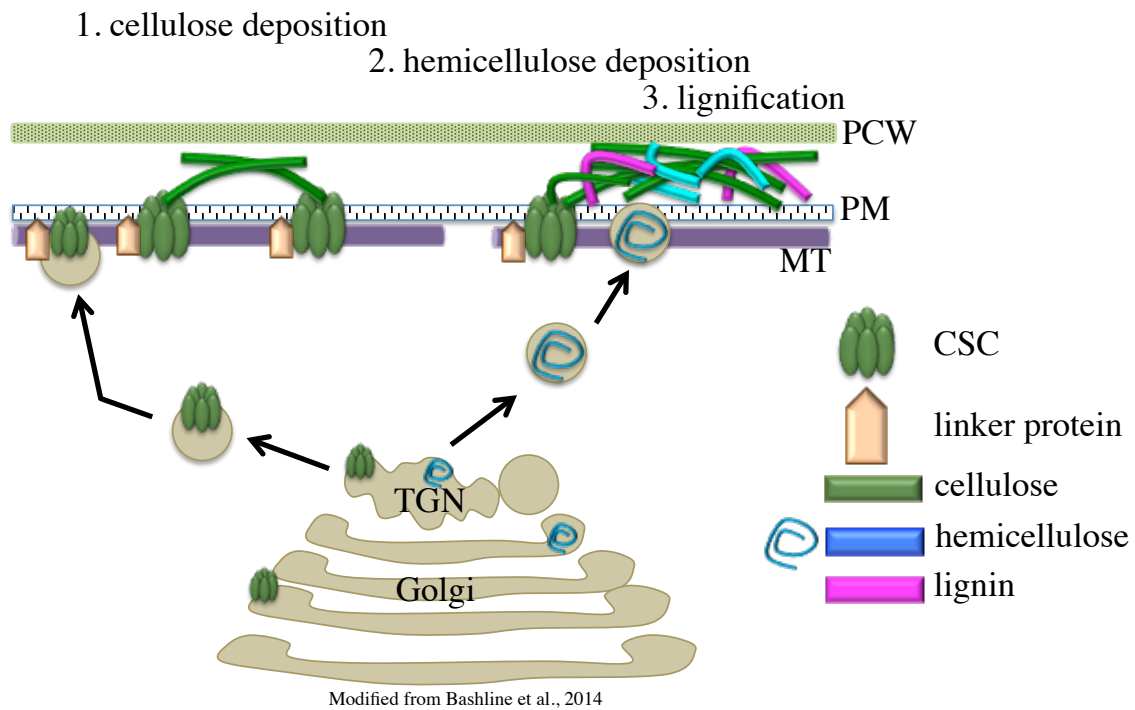


Figure 1. An overview of the general SCW deposition

Schematic diagram shows only key processes during SCW deposition. SCW is deposited between primary cell wall (PCW) and plasma membrane (PM). Firstly, cellulose synthase complex (CSC), probably assembled in Golgi, is transported and inserted into the PM. CSC interacts with cortical microtubules (MT) through linker proteins such as CSI1, and CSC deposits cellulose along microtubule tracks. Hemicellulose is synthesized in Golgi and secreted to cell wall domain. Upon hemicellulose association with cellulose, lignification occurs in the cell wall to form the mature rigid SCW.

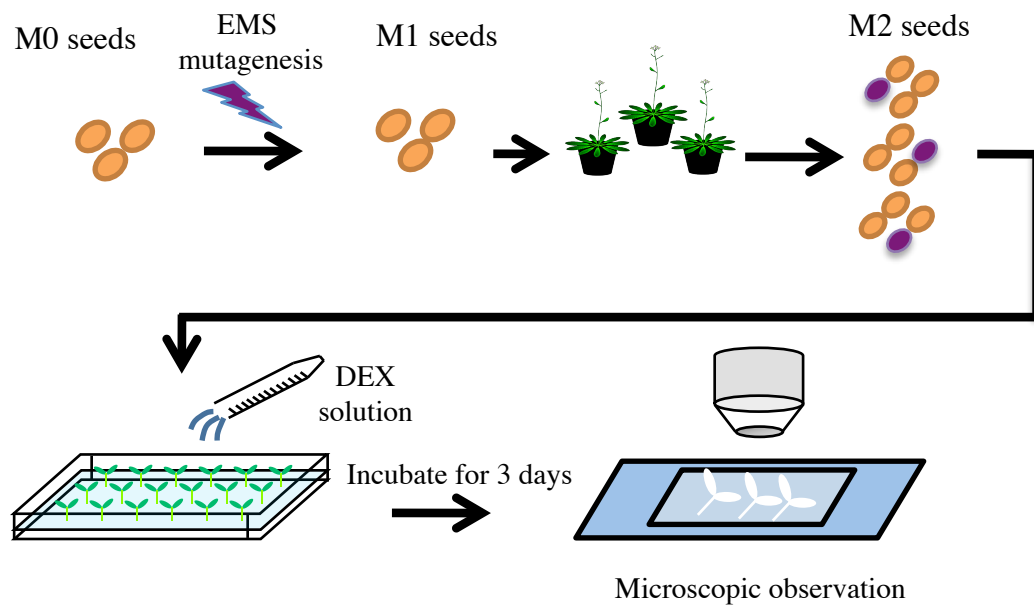


Figure 2. Scheme of genetic screening to isolate novel mutants related to SCW deposition

M0 seeds of *VND7-VP16-GR* were mutagenized with ethylmethanesulfonate to generate M1 seeds, and then M2 seeds were collected from each M1 plants independently. Six-day-old M2 seedlings were subjected to microscopic observation after 3-days of DEX treatment, to examine SCW deposition phenotypes.

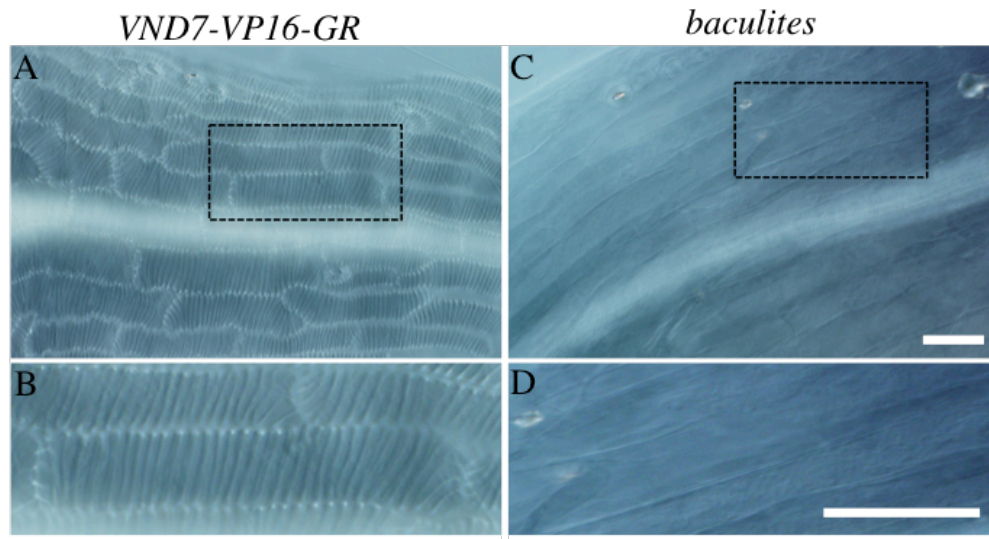


Figure 3. *baculites* is a mutant with loss of SCW patterning

(A-D) Differential interference contrast (DIC) images of wild-type *VND7-VP16-GR* (**A**, **B**) and *baculites VND7-VP16-GR* (**C**, **D**). Boxed area with black dot lines in (**A**) and (**C**) are enlarged in (**B**) and (**D**).

Bars = 100 μm .

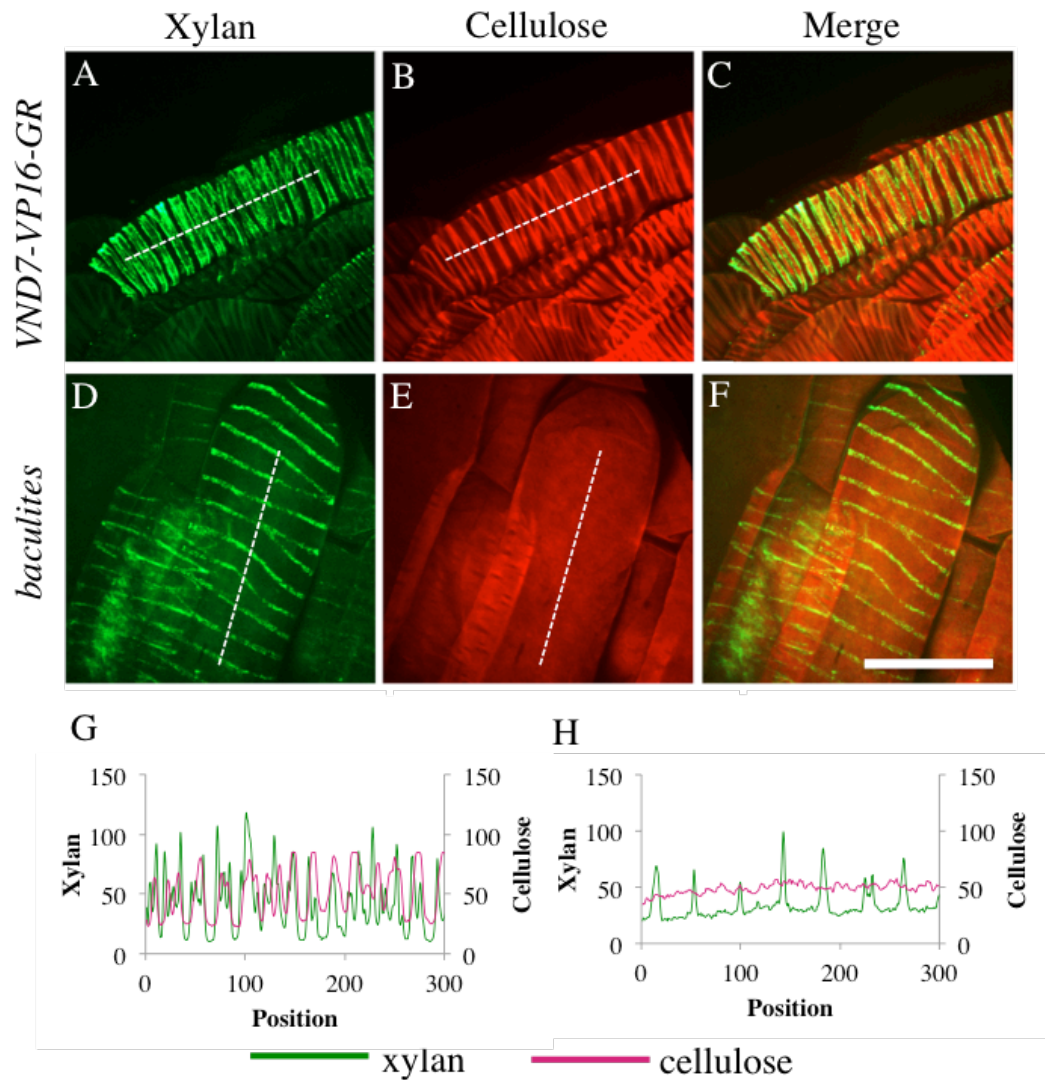


Figure 4. *baculites* has abnormality in cellulose deposition

(A-F) Visualization of cell wall components in wild-type *VND7-VP16-GR* (A, B, C) and *baculites VND7-VP16-GR* (D, E, F). Xylan was visualized by anti-xylan antibody LM10 (A, D), and cellulose was labeled with pontamine S4B (B, E). Merged views are shown in (C, F). The fluorescence signal intensities of xylan and cellulose along the white-dotted lines are shown in (G) and (H) respectively.

Bar = 30 μm .

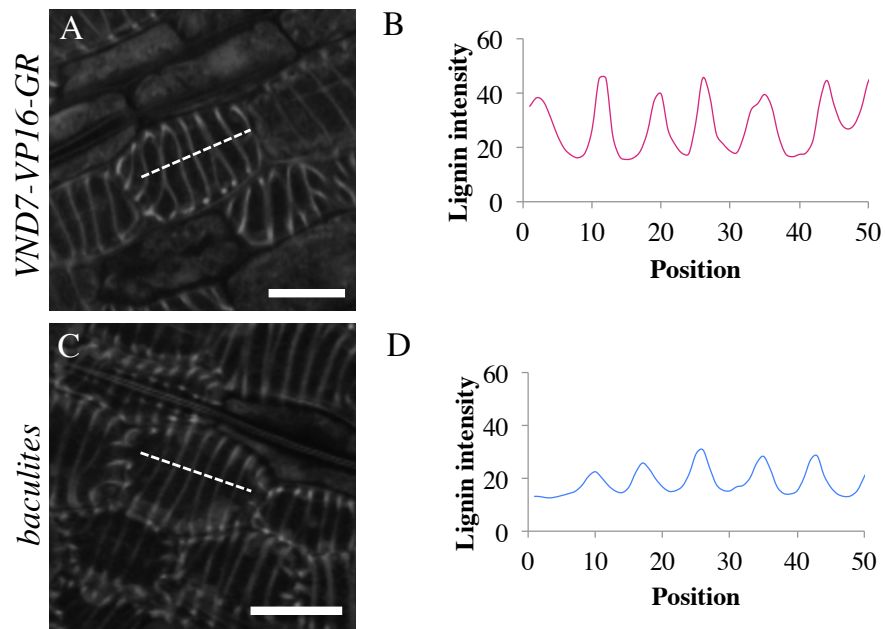


Figure 5. *baculites* has helical lignin accumulation

(A, C) Lignin autofluorescence in wild-type *VND7-VP16-GR* (A) and *baculites VND7-VP16-GR* (C). The fluorescence signal intensities along the dotted lines in (A) and (C) are shown in (B) and (D), respectively. Bars = 10 μm .



Figure 6. *baculites* is one of the *irregular xylem (irx)* mutants

(A-C) Transverse sections of root samples of 20-day-old plants of wild-type *VP16-GR* (A), wild-type *VND7-VP16-GR* (B), and *baculites VND7-VP16-GR* (C).

(D) Two-month-old plants of *VP16-GR* (left), *VND7-VP16-GR* (middle) and *baculites VND7-VP16-GR* (right).

Bars = 20 μm (A-C), 10 cm (D).

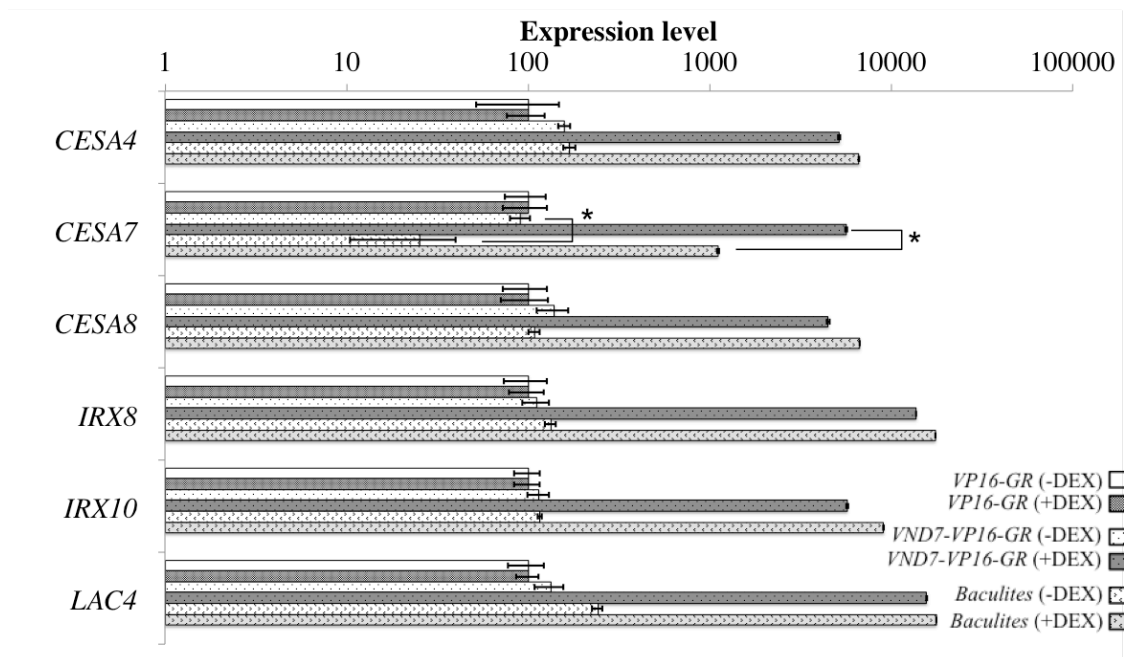


Figure 7. The *CESA7* expression is significantly decreased in *baculites*

Total RNA was extracted from 6-day-old seedlings of wild-type *VP16-GR*, wild-type *VND7-VP16-GR* and *baculites VND7-VP16-GR* treated with or without DEX. The *UBQ10* gene was used for the internal control, and the results were shown as relative values to the expression level in *VP16-GR* for each tested genes. Results are mean \pm SD (n=3). Statistically significant difference were found in the *CESA7* expression between wild-type *VND7-VP16-GR* and *baculites VND7-VP16-GR* (* $p < 0.05$; Student's t-test).

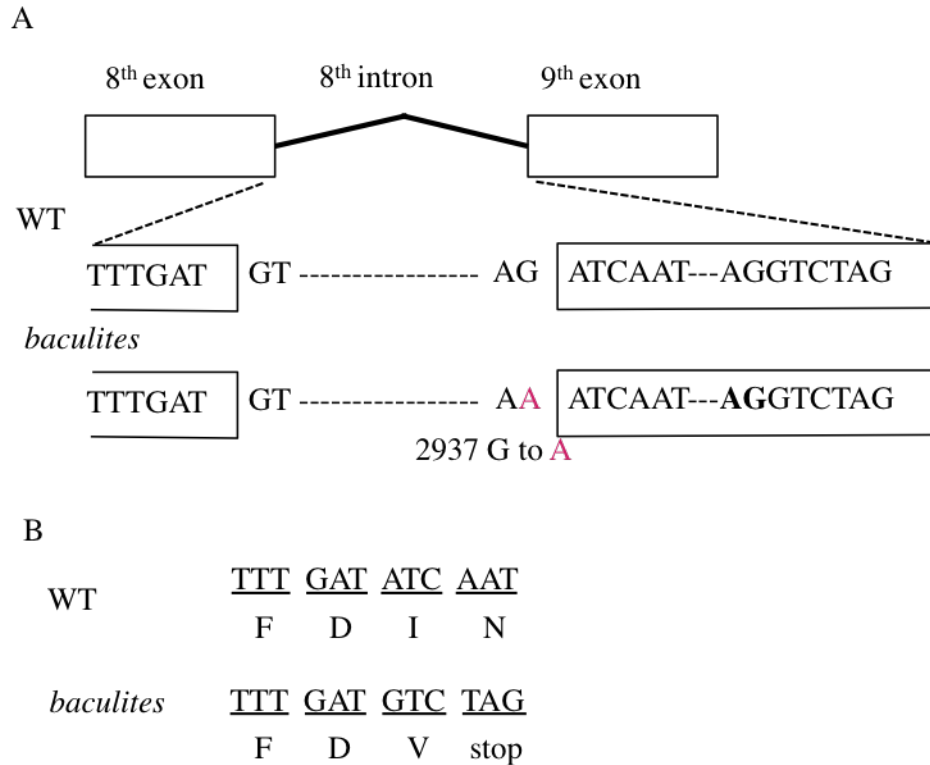


Figure 8. *baculites* has a single nucleotide substitution in the *CESA7* gene locus

(A) Single nucleotide substitution (G2937 to A transition, indicated in red) was found at the acceptor splice site of 8th intron of *CESA7* gene in the *baculites VND7-VP16-GR* genome, resulted in a shift to the next AG acceptor site, 13 bp downstream (indicated in bold).

(B) Change in the splice junction in (A) was predicted to produce the partial frame-shift and premature stop codon in *baculites VND7-VP16-GR*, a consequence confirmed by sequencing.

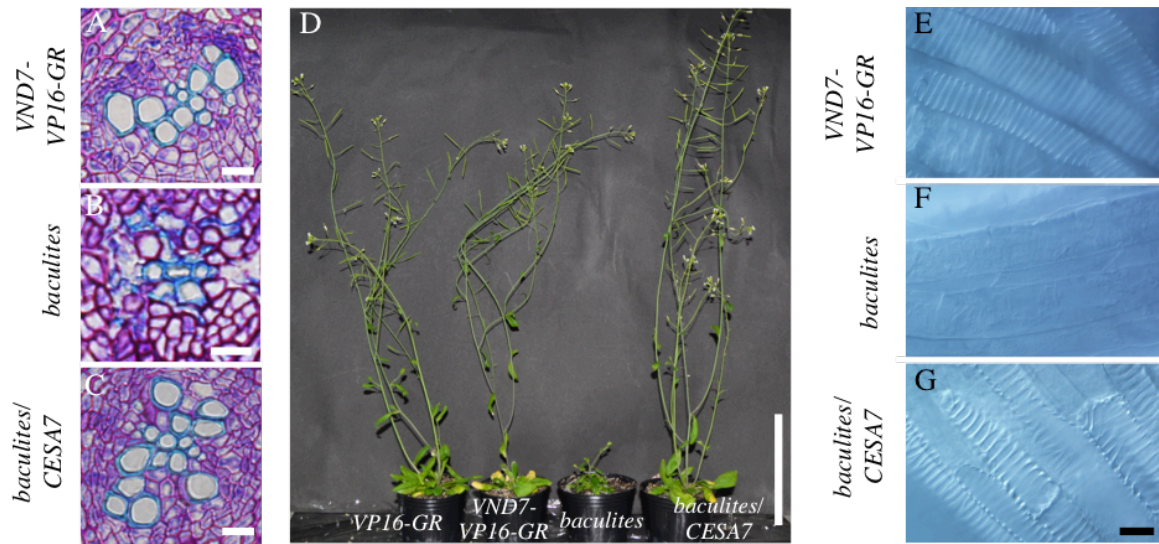


Figure 9. *CESA7* is the responsible gene for *baculites*

(A-C) Transverse sections of root samples of 20-day-old plants of wild-type VND7-VP16-GR (A), *baculites* VND7-VP16-GR (B) and *baculites* VND7-VP16-GR/*CESA7*pro::*YFP-CESA7* (C).

(D) Two-month-old plants of wild-type VP16-GR, wild-type VND7-VP16-GR, *baculites* VND7-VP16-GR, and *baculites* VND7-VP16-GR/*CESA7*pro::*YFP-CESA7*(left to right).

(E-G) DIC images of ectopically induced SCW in wild-type VND7-VP16-GR (E), *baculites* VND7-VP16-GR (F) and *baculites* VND7-VP16-GR/*CESA7*pro::*YFP-CESA7*(G).

Bars = 10 μm.

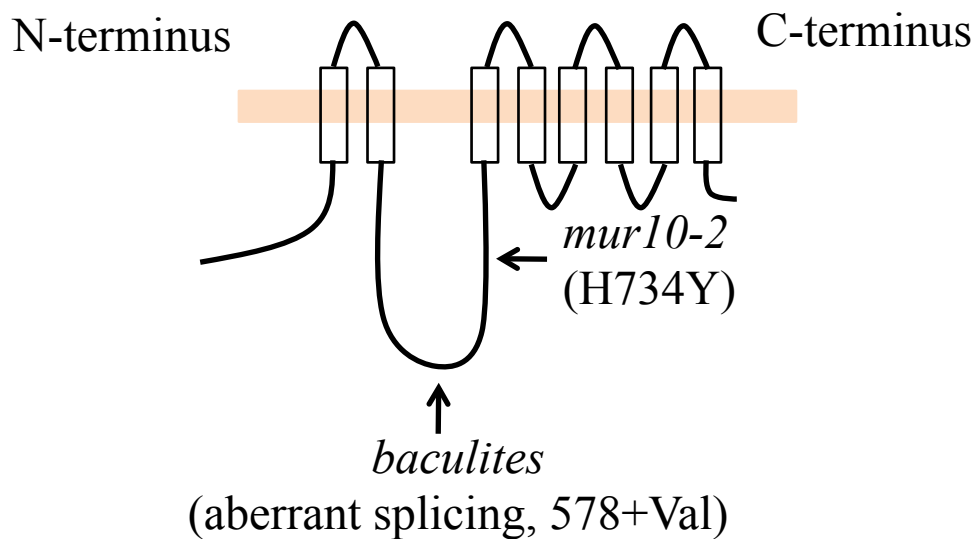


Figure 10. Schematic representation of CESA7 protein and positions of *baculites* and *mur10-2* mutations

Plant CESA proteins are predicted to contain eight transmembrane helices (indicated by open squares), the N terminal cytoplasmic domain, and the cytoplasmic domain located between the second and the third transmembrane helices. The positions of *mur10-2* and *baculites* mutations are shown.

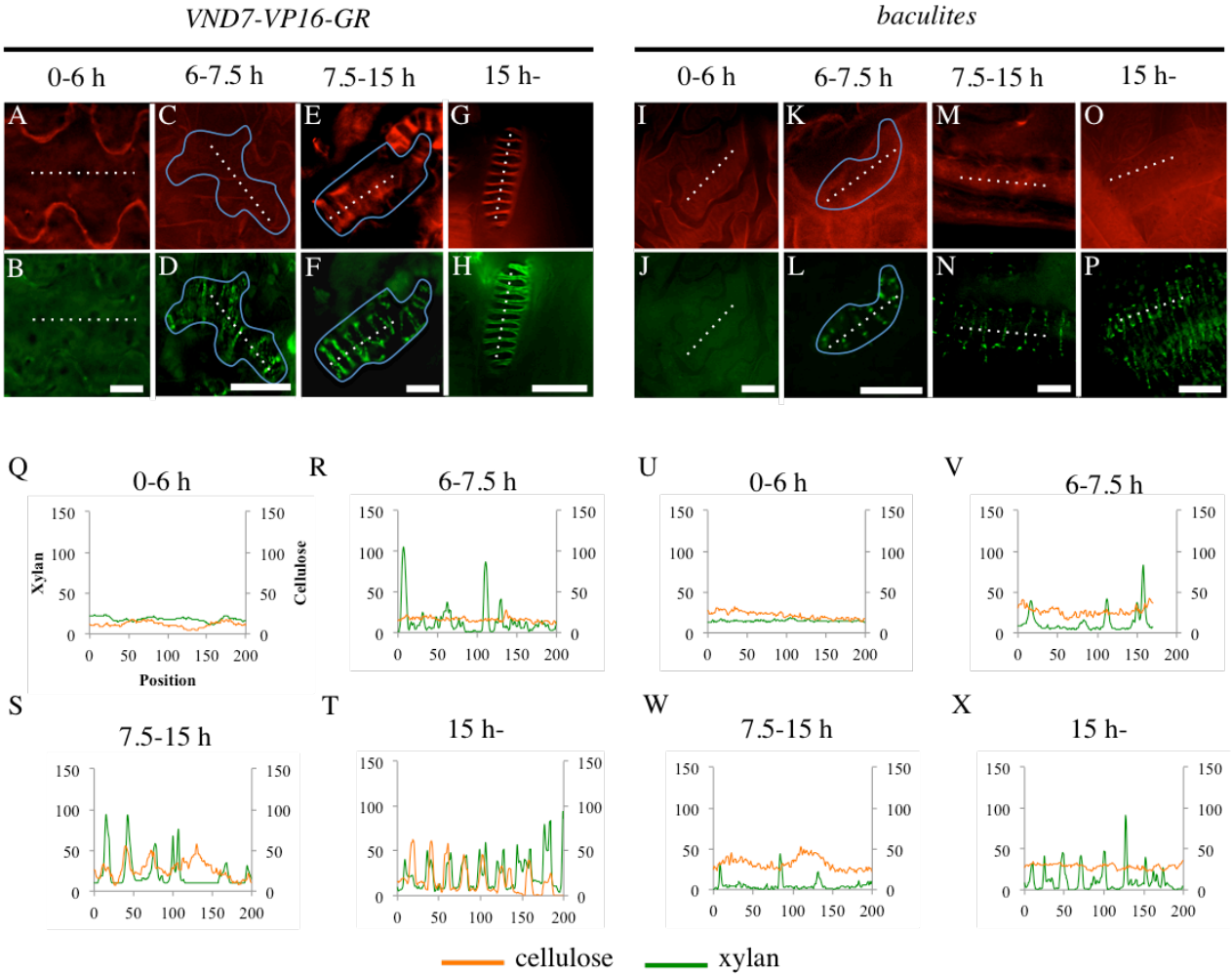


Figure 11. Xylan deposition was uncoupled with cellulose deposition at early stages of SCW formation

(A-P) Six-day-old seedlings of wild-type *VND7-VP16-GR* (A-H) and *baculites VND7-VP16-GR* (I-P) were treated with DEX, and sampled after 0-6 hours (A, B, I, J), 6-7.5 hours (C, D, K, L), 7.5-15 hours (E, F, M, N) and 15 hours (G, H, O, P) of DEX treatment. Cellulose (A, C, E, G, I, K, M, O) and xylan (B, D, F, H, J, L, N, P) were visualized with pontamine S4B and LM10 antibody.

(Q-X) The fluorescence signal intensities of cellulose and xylan along the white dotted lines in (A-P) are shown.

Bars = 10 μ m.

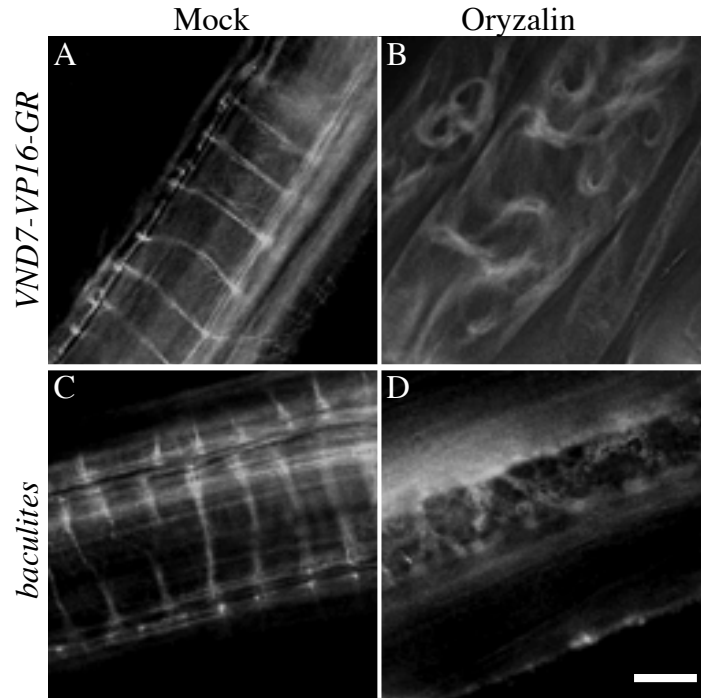


Figure 12. Cortical microtubule organization in *baculites* is similar to wild type

(A-D) Cortical microtubules were visualized by the introduction of *UBQ10pro::GFP-TUB6* into wild-type *VND7-VP16-GR* (A, B) and *baculites VND7-VP16-GR* (C, D). Helical arrangement of cortical microtubules were observed when protoxylem vessel cell differentiation (A, C), and the treatment with microtubule-depolymerizing drug, oryzalin disturbed such organizations in both of wild-type *VND7-VP16-GR* and *baculites VND7-VP16-GR* (B, D).

Bars = 10 μ m.

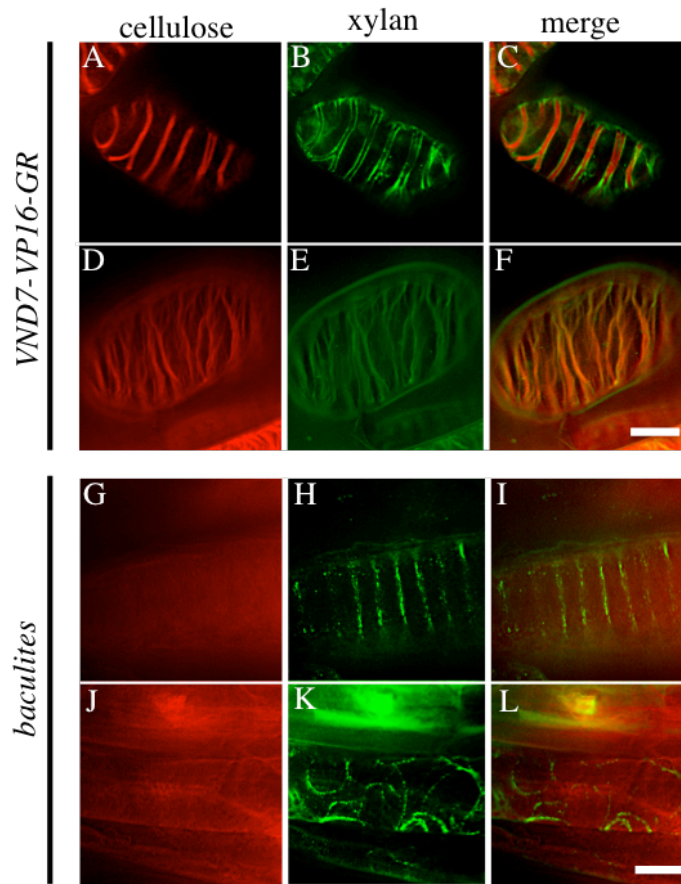


Figure 13. Patterned deposition of xylan is directed by cortical microtubules

(A-L) Six-day-old seedlings of wild-type *VND7-VP16-GR* (A-F) and *baculites VND7-VP16-GR* (G-L) were treated with only DEX (A-C, G-I) or both of DEX and oryzalin (D-F, J-L). Cellulose (A, D, G, J) and xylan (B, E, H, K) were visualized by pontamine S4B staining and immunostaining using LM10 antibody, respectively. Merged view of cellulose and xylan were shown in (C, F, I, L).

Bars = 10 μ m.

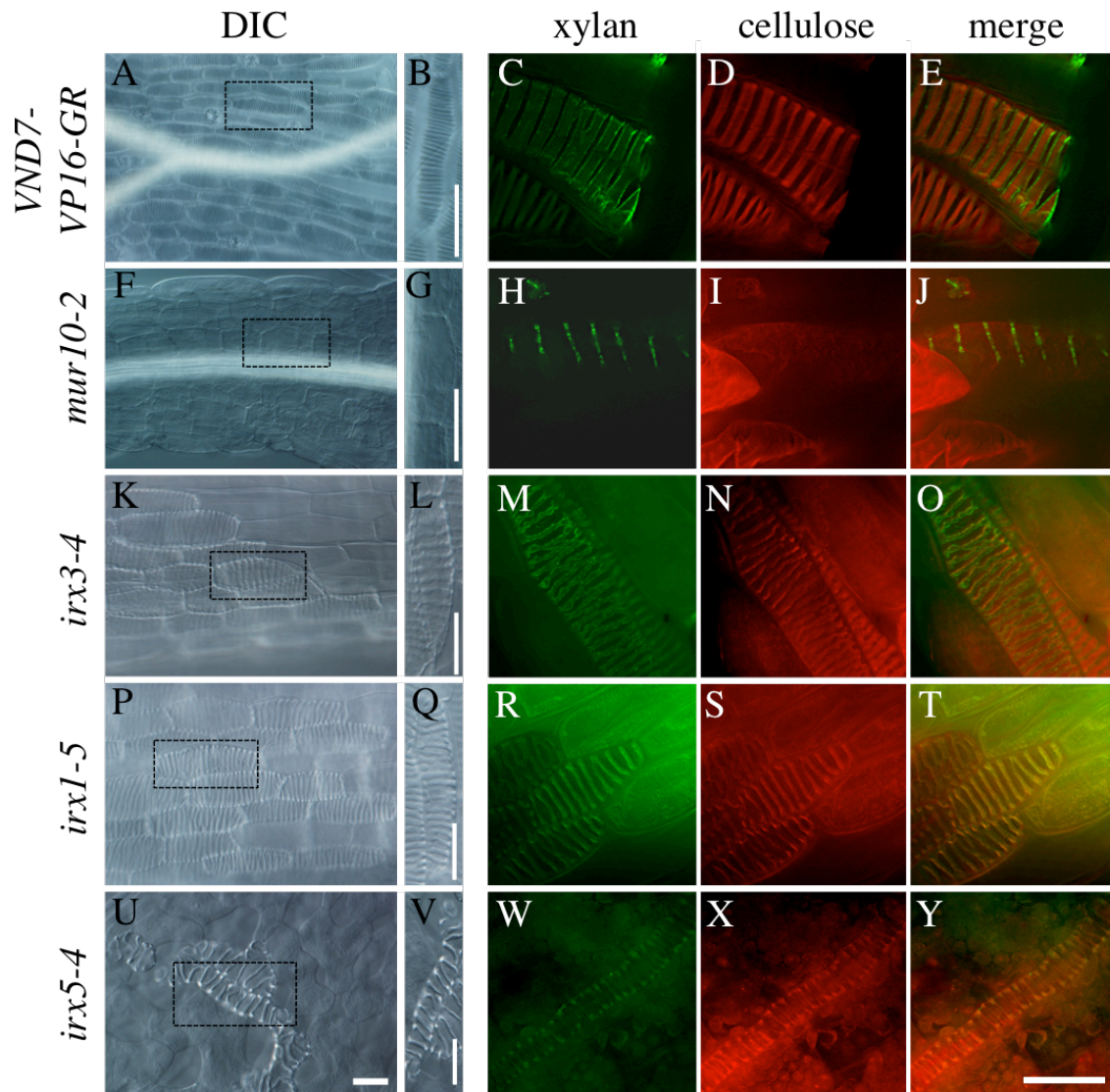


Figure 14. Mutations of SCW-type *CESA* genes differently affected SCW deposition during protoxylem vessel cell differentiation

Six-day-old seedlings with the *VND7-VP16-GR* construct in the following genotypes, wild type (A-E), *mur10-2/cesa7* (F-J), and *irx3-4/cesa7* (K-O), *irx1-5/cesa8* (P-T) and *irx5-4/cesa4* (U-Y), were treated with DEX to induce xylem vessel cell differentiation. DIC image was shown in (A, B, F, G, K, L, P, Q, U, V). Boxed area with black dot lines in (A, F, K, P, U) is close up in (B, G, L, Q, V). Xylan (C, H, M, R, W) and cellulose (D, I, N, S, X) were visualized by immunostaining using LM10 antibody and pontamine S4B staining, respectively. Merged view of xylan and cellulose were shown in (E, J, O, T, Y).

Bars = 50 μ m (A, B, F, G, K, L, P, Q, U, V), 20 μ m (C, D, E, H, I, J, M, N, O, R, S, T, W, X, Y).

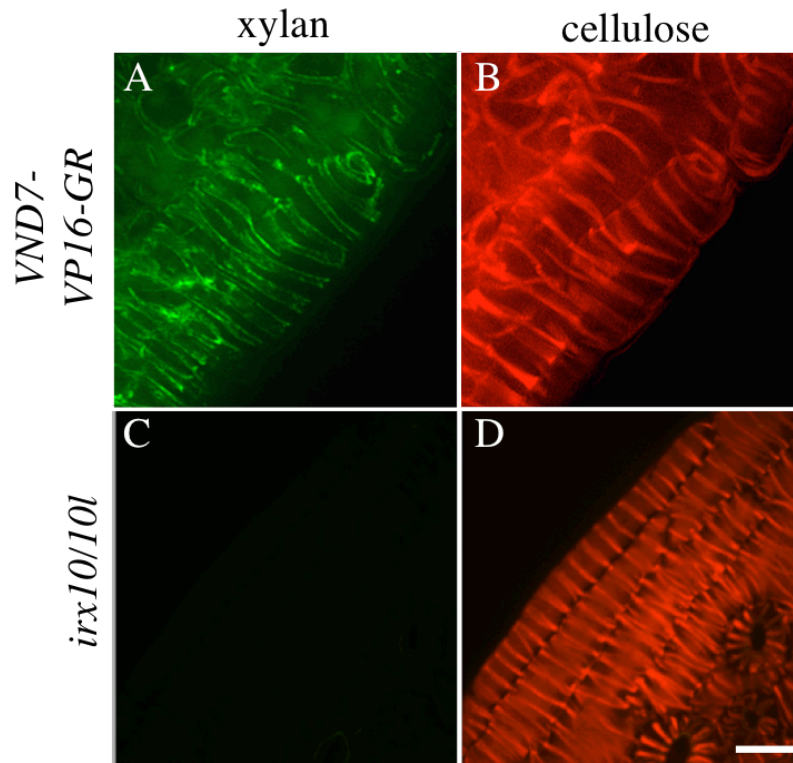


Figure 15. Defects in xylan synthesis did not affect the patterned cellulose deposition

Six-day-old seedlings of wild-type *VND7-VP16-GR* (**A, B**) and the double mutant *irx10 irx10l* (*irx10/10l*) with *UBQ10pro::VND7-VP16-GR* (**C, D**) were treated with DEX. Xylan (**A, C**) and cellulose (**B, D**) were visualized by immunostaining using LM10 antibody and pontamine S4B staining, respectively. Bar = 20 μ m.

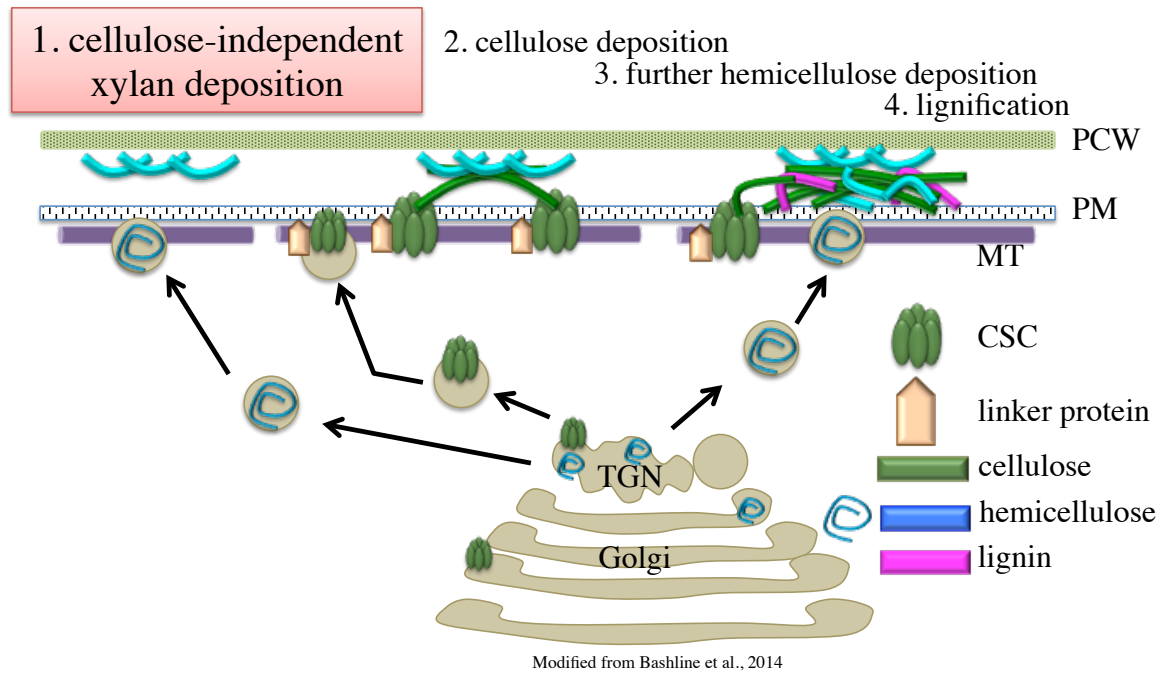


Figure 16. A proposed model for the SCW deposition during protoxylem vessel cells based on the results presented in this thesis

Considering the obtained results here, I propose that SCW deposition might start with microtubule (MT)-directed xylan deposition followed by the cellulose deposition by cellulose synthase complex (CSC). Subsequently, further deposition of hemicellulose and lignin would occur to form rigid SCW, during protoxylem vessel cell formation in Arabidopsis.

PCW: primary cell wall, PM: plasma membrane, TGN: trans Golgi network

6. Acknowledgements

I am very grateful to Prof. Taku Demura for the continuous support, guidance and critical discussion on my study. He has been supportive since I was Master course student.

I deeply appreciate Assistant Prof. Misato Ohtani for the perfect guidance through all these years. Her continuous cooperation helped me a lot to accomplish research including experiment and manuscript writing.

I want to express special thanks to Dr. Mathias Schuetz and Prof. Lacey Samuels in University of British Columbia for helping to perform microscopic work and manuscript writing.

I also want to thank Mr. Yoichiro Watanabe, Ms. Miranda. J. Meents and Ms. Eva Chou for helping me to perform experiments in University of British Columbia.

I would like to show my gratitude to Associate Prof. Minoru Kubo, Assistant Prof. Arata Yoneda, Assistant Prof. Ko Kato, Dr. Ryosuke Sano, Dr. Hitoshi Endo and Mr. Harunori Kawabe for critical discussion, technical and continuous supports.

I thank advisors, Prof. Masao Tasaka and Prof. Keiji Nakajima for critical discussion on my research.

Lastly, I am grateful for all members in Demura Laboratory.

7. References

- Alejandro, S., Lee, Y., Tohge, T., Sudre, D., Osorio, S., Park, J., Bovet, L., Lee, Y., Geldner, N., Fernie, A.R., and Martinoia, E.** (2012). AtABCG29 is a monolignol transporter involved in lignin biosynthesis. *Curr. Biol.* **22**: 1207–1212.
- Anderson, C.T., Carroll, A., Akhmetova, L., and Somerville, C.** (2010). Real-time imaging of cellulose reorientation during cell wall expansion in Arabidopsis roots. *Plant Physiol.* **152**: 787–796.
- Awano, T., Takabe, K., and Fujita, M.** (1998). Localization of glucuronoxylans in Japanese beech visualized by immunogold labelling. *Protoplasma.* **202**: 213–222.
- Balakshin, M., Capanema, E., Gracz, H., Chang, H.M., and Jameel, H.** (2011). Quantification of lignin-carbohydrate linkages with high-resolution NMR spectroscopy. *Planta.* **233**: 1097–1110.
- Berthet, S., Demont-Caulet, N., Pollet, B., Bidzinski, P., Cézard, L., Le Bris, P., Borrega, N., Hervé, J., Blondet, E., Balzergue, S., Lapierre, C., and Jouanin, L.** (2011). Disruption of LACCASE4 and 17 results in tissue-specific alterations to lignification of Arabidopsis thaliana stems. *Plant Cell.* **23**: 1124–1137.
- Bonawitz, N.D. and Chapple, C.** (2010). The genetics of lignin biosynthesis: connecting genotype to phenotype. *Annu. Rev. Genet.* **44**: 337–363.
- Bosca, S., Barton, C.J., Taylor, N.G., Ryden, P., Neumetzler, L., Pauly, M., Roberts, K., and Seifert, G.J.** (2006). Interactions between MUR10/CesA7-dependent secondary cellulose biosynthesis and primary cell wall structure. *Plant Physiol.* **142**: 1353–1363.
- Bringmann, M., Li, E., Sampathkumar, A., Kocabek, T., Hauser, M.T., and Persson, S.** (2012). POM-POM2/CELLULOSE SYNTHASE INTERACTING1 is essential for the functional association of cellulose synthase and microtubules in Arabidopsis. *Plant Cell.* **24**: 163–177.
- Bromley, J.R., Busse-Wicher, M., Tryfona, T., Mortimer, J.C., Zhang, Z., Brown, D.M., and Dupree, P.** (2013). GUX1 and GUX2 glucuronyltransferases decorate distinct domains of glucuronoxylan with different substitution patterns. *Plant J.* **74**: 423–434.
- Brown, D., Wightman, R., Zhang, Z., Gomez, L.D., Atanassov, I., Bukowski, J.P., Tryfona, T., McQueen-Mason, S.J., Dupree, P., and Turner, S.R.** (2011). Arabidopsis genes IRREGULAR XYLEM (IRX15) and IRX15L encode DUF579-containing proteins that are essential for normal xylan deposition in the secondary cell wall. *Plant J.* **66**: 401–413.

- Brown, D.M., Zeef, L.A.H., Ellis, J., Goodacre, R., and Turner, S.R.** (2005). Identification of novel genes in arabidopsis involved in secondary cell wall formation using expression profiling and reverse genetics. *Plant Cell*. **17**: 2281–2295.
- Brown, D.M., Zhang, Z., Stephens, E., Dupree, P., and Turner, S.R.** (2009). Characterization of IRX10 and IRX10-like reveals an essential role in glucuronoxylan biosynthesis in Arabidopsis. *Plant J*. **57**: 732–746.
- Busse-Wicher, M., Gomes, T.C.F., Tryfona, T., Nikolovski, N., Stott, K., Grantham, N.J., Bolam, D.N., Skaf, M.S., and Dupree, P.** (2014). The pattern of xylan acetylation suggests xylan may interact with cellulose microfibrils as a twofold helical screw in the secondary plant cell wall of *Arabidopsis thaliana*. *Plant J*. **79**: 492–506.
- Cosgrove, D.J. and Jarvis, M.C.** (2012). Comparative structure and biomechanics of plant primary and secondary cell walls. *Front. Plant Sci*. **3**: 1–6.
- Crowell, E.F., Gonneau, M., Stierhof, Y.D., Höfte, H., and Vernhettes, S.** (2010). Regulated trafficking of cellulose synthases. *Curr. Opin. Plant Biol*. **13**: 700–705.
- Delmer, D.P.** (1999). Cellulose biosynthesis: exciting times for a difficult field of study. *Annu. Rev. Plant Physiol. Plant Mol. Biol*. **50**: 245–276.
- Demura, T., Tashiro, G., Horiguchi, G., Kishimoto, N., Kubo, M., Matsuoka, N., Minami, A., Nagata-Hiwatashi, K., Nakamura, K., Okamura, Y., Sassa, N., Suzuki, S., Yazaki, J., Kikuchi, S., and Fukuda, H.** (2002). Visualization by comprehensive microarray analysis of gene expression programs during transdifferentiation of mesophyll cells into xylem cells. *Proc. Natl. Acad. Sci. USA*. **99**: 15794–15799.
- Derba-Maceluch, M., Awano, T., Takahashi, J., Lucenius, J., Ratke, C., Kontro, I., Busse-Wicher, M., Kosik, O., Tanaka, R., Winzell, A., Kallas, A., Leśniewska, J., Berthold, F., immerzeel, P., Teeri, T.T., Ezcurra, I., Dupree, P., Serimaa, R., and Mellerowicz, E.J.** (2015). Suppression of xylan endotransglycosylase PtxtXyn10A affects cellulose microfibril angle in secondary wall in aspen wood. *New Phytol*. **205**: 666–81.
- Derbyshire, P., Ménard, D., Green, P., Saalbach, G., Buschmann, H., Lloyd, C.W., and Pesquet, E.** (2015). Proteomic analysis of microtubule interacting proteins over the course of xylem tracheary element formation in Arabidopsis. *Plant Cell*. **27**: 2709–2726
- Donaldson, L.A. and Knox, J.P.** (2012). Localization of cell wall polysaccharides in normal and compression wood of radiata pine: Relationships with lignification and microfibril orientation. *Plant Physiol*. **158**: 642–653.

- Dupree, P., and Sherrier, D.J.** (1998). The plant Golgi apparatus. *Biochim. Biophys. Acta. Mol. Cell. Res.* **1404**: 259–270.
- Endler, A., Kesten, C., Schneider, R., Zhang, Y., Ivakov, A., Froehlich, A., Funke, N., and Persson, S.** (2015). A mechanism for sustained cellulose synthesis during salt stress. *Cell.* **162**: 1353–1364.
- Endo, S., Pesquet, E., Yamaguchi, M., Tashiro, G., Sato, M., Toyooka, K., Nishikubo, N., Udagawa-Motose, M., Kubo, M., Fukuda, H., and Demura, T.** (2009). Identifying new components participating in the secondary cell wall formation of vessel elements in zinnia and Arabidopsis. *Plant Cell.* **21**: 1155–1165.
- Faik, A.** (2010). Xylan Biosynthesis: News from the Grass. *Plant Physiol.* **153**: 396–402.
- Fukuda, H., and Komamine, A.** (1980). Establishment of an experimental system for the study of tracheary element differentiation from single cells isolated from the mesophyll of zinnia elegans. *Plant Physiol.* **65**: 57–60.
- Greco, M., Chiappetta, A., Bruno, L., and Bitonti, M.B.** (2012). In *Posidonia oceanica* cadmium induces changes in DNA methylation and chromatin patterning. *J. Exp. Bot.* **63**: 695–709.
- Gu, Y., Kaplinsky, N., Bringmann, M., Cobb, A., Carroll, A., Sampathkumar, A., Baskin, T.I., Persson, S., and Somerville, C.R.** (2010). Identification of a cellulose synthase-associated protein required for cellulose biosynthesis. *Proc. Natl. Acad. Sci. USA.* **107**: 12866–12871.
- Guerriero, G., Fugelstad, J., and Bulone, V.** (2010). What do we really know about cellulose biosynthesis in higher plants? *J. Integr. Plant Biol.* **52**: 161–175.
- Gutierrez, R., Lindeboom, J.J., Paredez, A.R., Emons, A.M.C., and Ehrhardt, D.W.** (2009). Arabidopsis cortical microtubules position cellulose synthase delivery to the plasma membrane and interact with cellulose synthase trafficking compartments. *Nat. Cell Biol.* **11**: 797–806.
- Hamant, O. and Traas, J.** (2010). The mechanics behind plant development. *New Phytol.* **185**: 369–385.
- Hepler, P., Fosket, D., and Newcomb, E.** (1970). Lignification During Secondary Wall Formation in Coleus: An Electron Microscopic Study. *Am. J. Bot.* **57**: 85-96
- Hogetsu, T.** (1990). Detection of hemicelluloses specific to the cell wall of tracheary elements and phloem cells by fluorescein-conjugated lectins. *Protoplasma.* **156**: 67–73.

- Jensen, J.K., Kim, H., Cocuron, J.C., Orlor, R., Ralph, J., and Wilkerson, C.G.** (2011). The DUF579 domain containing proteins IRX15 and IRX15-L affect xylan synthesis in Arabidopsis. *Plant J.* **66**: 387–400.
- Jones, L., Ennos, a R., and Turner, S.R.** (2001). Cloning and characterization of *irregular xylem4 (irx4)*: A severely lignin-deficient mutant of Arabidopsis. *Plant J.* **26**: 205–216.
- Kubo, M., Udagawa, M., Nishikubo, N., Horiguchi, G., Yamaguchi, M., Ito, J., Mimura, T., Fukuda, H., and Demura, T.** (2005). Transcription switches for protoxylem and metaxylem vessel formation. *Genes Dev.* **19**: 1855–1860.
- Lee, C., Zhong, R., Richardson, E., Himmelsbach, D.S., McPhail, B.T., and Ye, Z.H.** (2007). The PARVUS gene is expressed in cells undergoing secondary wall thickening and is essential for glucuronoxylan biosynthesis. *Plant Cell Physiol.* **48**: 1659–1672.
- Leszek, A.** (2002). Compatibilization of Polymer Blends. *Can. J. Chem. Eng.* **80**: 1008–1016.
- Li, S., Lei, L., Yingling, Y.G., and Gu, Y.** (2015). Microtubules and cellulose biosynthesis: the emergence of new players. *Curr. Opin. Plant Biol.* **28**: 76–82.
- McCartney, L., Marcus, S.E., and Knox, J.P.** (2005). Monoclonal antibodies to plant cell wall xylans and arabinoxylans. *J. Histochem. Cytochem.* **53**: 543–546.
- McFarlane, H.E., Döring, A., and Persson, S.** (2014). The cell biology of cellulose synthesis. *Annu. Rev. Plant Biol.* **65**: 69–94.
- Miao, Y.C., and Liu, C.J.** (2010). ATP-binding cassette-like transporters are involved in the transport of lignin precursors across plasma and vacuolar membranes. *Proc. Natl. Acad. Sci. USA.* **107**: 22728–22733.
- Mortimer, J.C., Miles, G.P., Brown, D.M., Zhang, Z., Segura, M.P., Weimar, T., Yu, X., Seffen, K., Stephens, E., Turner, S.R., and Dupree, P.** (2010). Absence of branches from xylan in Arabidopsis *gux* mutants reveals potential for simplification of lignocellulosic biomass. *Proc. Natl. Acad. Sci. USA.* **107**: 17409–17414.
- Mueller, S.C., Brown, M., and Scott, T.** (1976). Cellulosic Microfibrils: Nascent Stages of Synthesis in a Higher Plant Cell. *Science.* **194**: 949–951.
- Myburg, A.A., Lev - Yadun, S., and Sederoff, R.R.** (2013). Xylem structure and function. *eLS*: 1–19.

- Nakamura, M., Naoi, K., Shoji, T., and Hashimoto, T.** (2004). Low concentrations of propyzamide and oryzalin alter microtubule dynamics in Arabidopsis epidermal cells. *Plant Cell Physiol.* **45**: 1330–1334.
- Nakano, Y., Yamaguchi, M., Endo, H., Rejab, N.A., and Ohtani, M.** (2015). NAC-MYB-based transcriptional regulation of secondary cell wall biosynthesis in land plants. *Front. Plant Sci.* **6**: 1–18.
- Northcote, D.H., Davey, R., and Lay, J.** (1989). Planta in the cell-plate, primary and secondary walls of plant cells. *Planta.* **178**: 353–366.
- Northcote, D.H. and Pickett-Heaps, J.D.** (1966). A function of the Golgi apparatus in polysaccharide synthesis and transport in the root-cap cells of wheat. *Biochem. J.* **98**: 159–167.
- Oda, Y. and Fukuda, H.** (2012). Initiation of cell wall pattern by a rho- and microtubule-driven symmetry breaking. *Science.* **337**: 1333–1336.
- Oda, Y. and Fukuda, H.** (2013). Rho of plant GTPase signaling regulates the behavior of Arabidopsis Kinesin-13A to establish secondary cell wall patterns. *Plant Cell.* **25**: 4439–4450.
- Oda, Y., Iida, Y., Kondo, Y., and Fukuda, H.** (2010). Wood cell-wall structure requires local 2D-microtubule disassembly by a novel plasma membrane-anchored protein. *Curr. Biol.* **20**: 1197–1202.
- Oda, Y., Mimura, T., and Hasezawa, S.** (2005). Regulation of secondary cell wall development by cortical microtubules during tracheary element differentiation in Arabidopsis cell suspensions. *Plant Physiol.* **137**: 1027–1036.
- Pauly, M. and Keegstra, K.** (2008). Cell-wall carbohydrates and their modification as a resource for biofuels. *Plant J.* **54**: 559–568.
- Pear, J.R., Kawagoe, Y., Schreckengost, W.E., Delmer, D.P., and Stalker, D.M.** (1996). Higher plants contain homologs of the bacterial celA genes encoding the catalytic subunit of cellulose synthase. *Proc. Natl. Acad. Sci. USA.* **93**: 12637–12642.
- Peña, M.J., Zhong, R., Zhou, G.K., Richardson, E., O'Neill, M., Darvill, A.G., York, W.S., and Ye, Z.H.** (2007). Arabidopsis *irregular xylem8* and *irregular xylem9*: implications for the complexity of glucuronoxylan biosynthesis. *Plant Cell.* **19**: 549–563.
- Persson, S., Caffall, K.H., Freshour, G., Hilley, M.T., Bauer, S., Poindexter, P., Hahn, M.G., Mohnen, D., and Somerville, C.** (2007). The Arabidopsis *irregular xylem8* mutant is deficient in glucuronoxylan and homogalacturonan, which are essential for secondary cell wall integrity. *Plant Cell.* **19**: 237–55.

- Pesquet, E., Korolev, A.V, Calder, G., and Lloyd, C.W.** (2010). The microtubule-associated protein AtMAP70-5 regulates secondary wall patterning in Arabidopsis wood cells. *Curr. Biol.* **20**: 744–749.
- Ray, P.M.** (1967). Radioautographic study of cell wall deposition in growing plant cells. *J. Cell Biol.* **35**: 659–74.
- Reis, D., and Vian, B.** (2004). Helicoidal pattern in secondary cell walls and possible role of xylans in their construction. *Comptes Rendus Biol.* **327**: 785–790.
- Reiter, W.D., Chapple, C., and Somerville, C.R.** (1997). Mutants of Arabidopsis thaliana with altered cell wall polysaccharide composition. *Plant J.* **12**: 335–345.
- Rejab, N.A., Nakano, Y., Yoneda, A., Ohtani, M., and Demura, T.** (2015). Possible contribution of TED6 and TED7, secondary cell wall-related membrane proteins, to evolution of tracheary element in angiosperm lineage. *Plant Biotechnol.* **32**: 343–347.
- Rennie, E., Hansen, S.F., Baidoo, E.E.K., Hadi, M.Z., Keasling, J.D., and Scheller, H. V.** (2012). Three Members of the Arabidopsis Glycosyltransferase Family 8 Are Xylan Glucuronosyltransferases. *Plant Physiol.* **159**: 1408–1417.
- Scheller, H.V. and Ulvskov, P.** (2010). Hemicelluloses. *Annu. Rev. Plant Biol.* **61**: 263–289.
- Schuetz, M., Benske, A., Smith, R.A., Watanabe, Y., Tobimatsu, Y., Ralph, J., Demura, T., Ellis, B., and Samuels, A.L.** (2014). Laccases direct lignification in the discrete secondary cell wall domains of protoxylem. *Plant Physiol.* **166**: 798–807.
- Taylor, N.G., Scheible, W.R., Cutler, S., Somerville, C.R., and Turner, S.R.** (1999). The *irregular xylem3* locus of Arabidopsis encodes a cellulose synthase required for secondary cell wall synthesis. *Plant Cell.* **11**: 769–780.
- Terashima, N. and Fukushima, K.** (1988). Heterogeneity in formation of lignin-XI: An autoradiographic study of the heterogeneous formation and structure of pine lignin. *Wood Sci. Technol.* **22**: 259–270.
- Tsuyama, T., Kawai, R., Shitan, N., Matoh, T., Sugiyama, J., Yoshinaga, A., Takabe, K., Fujita, M., and Yazaki, K.** (2013). Proton-dependent coniferin transport, a common major transport event in differentiating xylem tissue of woody plants. *Plant Physiol.* **162**: 918–26.
- Turner, S.R. and Somerville, C.R.** (1997). Collapsed xylem phenotype of Arabidopsis identifies mutants deficient in cellulose deposition in the secondary cell wall. *Plant Cell.* **9**: 689–701.

- Vain, T., Crowell, E.F., Timpano, H., Biot, E., Desprez, T., Mansoori, N., Trindade, L.M., Pagant, S., Robert, S., Höfte, H., Gonneau, M., and Vernhettes, S.** (2014). The cellulase KORRIGAN is part of the cellulose synthase complex. *Plant Physiol.* **165**: 1521–1532.
- Vandavasi, V.G., Putnam, D.K., Zhang, Q., Petridis, L., Heller, W.T., Tracy Nixon, B., Haigler, C.H., Kalluri, U., Coates, L., Langan, P., Smith, J.C., Meiler, J., and O'Neill, H.** (2015). A structural study of CESA1 catalytic domain of *Arabidopsis thaliana* cellulose synthesis complex: evidence for CESA trimers. *Plant Physiol.* **170**: 123–135
- Vanholme, R., Demedts, B., Morreel, K., Ralph, J., and Boerjan, W.** (2010). Lignin biosynthesis and structure. *Plant Physiol.* **153**: 895–905.
- Wang, Y., Chantreau, M., Sibout, R., and Hawkins, S.** (2013). Plant cell wall lignification and monolignol metabolism. *Front. Plant Sci.* **4**: 1–14.
- Watanabe, Y., Meents, M.J., McDonnell, M.J., Barkwil, S., Sampathkumar, A., Cartwright, H.N., Demura, T., Ehrhardt, D.E., Samuels, A.L., and Mansfield, S.D.** (2015). Visualization of cellulose synthases in *Arabidopsis* secondary cell walls. *Science.* **350**: 198–203.
- Wightman, R. and Turner, S.R.** (2008). The roles of the cytoskeleton during cellulose deposition at the secondary cell wall. *Plant J.* **54**: 794–805.
- Wolf, S., Hématy, K., and Höfte, H.** (2012). Growth control and cell wall signaling in plants. *Annu. Rev. Plant Biol.* **63**: 381–407.
- Wu, A.M., Hörnblad, E., Voxeur, A., Gerber, L., Rihouey, C., Lerouge, P., and Marchant, A.** (2010). Analysis of the *Arabidopsis* IRX9/IRX9-L and IRX14/IRX14-L pairs of glycosyltransferase genes reveals critical contributions to biosynthesis of the hemicellulose glucuronoxylan. *Plant Physiol.* **153**: 542–554.
- Wu, A.M., Rihouey, C., Seveno, M., Hörnblad, E., Singh, S.K., Matsunaga, T., Ishii, T., Lerouge, P., and Marchant, A.** (2009). The *Arabidopsis* IRX10 and IRX10-LIKE glycosyltransferases are critical for glucuronoxylan biosynthesis during secondary cell wall formation. *Plant J.* **57**: 718–731.
- Xu, B., Ohtani, M., Yamaguchi, M., Toyooka, K., Wakazaki, M., Sato, M., Kubo, M., Nakano, Y., Sano, R., Hiwatashi, Y., Murata, T., Kurata, T., Yoneda, A., Hasebe, M., and Demura, T.** (2014). Contribution of NAC transcription factors to plant adaptation to land. *Science.* **343**: 1505–1508.
- Yamaguchi, M., Goué, N., Igarashi, H., Ohtani, M., Nakano, Y., Mortimer, J.C., Nishikubo, N., Kubo, M., Katayama, Y., Kakegawa, K., Dupree, P., and Demura, T.** (2010). VASCULAR-RELATED NAC-DOMAIN6 and VASCULAR-

RELATED NAC-DOMAIN7 effectively induce transdifferentiation into xylem vessel elements under control of an induction system. *Plant Physiol.* **153**: 906–914.

Yuan, T.Q., Sun, S.N., Xu, F., and Sun, R.C. (2011). Characterization of lignin structures and lignin-carbohydrate complex (LCC) linkages by quantitative ¹³C and 2D HSQC NMR spectroscopy. *J. Agric. Food Chem.* **59**: 10604–10614.

Zhao, Q., Nakashima, J., Chen, F., Yin, Y., Fu, C., Yun, J., Shao, H., Wang, X., Wang, Z.Y., and Dixon, R.A. (2013). Laccase is necessary and nonredundant with peroxidase for lignin polymerization during vascular development in Arabidopsis. *Plant Cell.* **25**: 3976–87.

Zhong, R., Morrison, W.H., Freshour, G.D., Hahn, M.G., and Ye, Z.H. (2003). Expression of a mutant form of cellulose synthase AtCesA7 causes dominant negative effect on cellulose biosynthesis. *Plant Physiol.* **132**: 786–795.

Zhou, G., Nairn, C.J., Wood-jones, A., Richardson, E., Zhong, R., and Pen, M.J. (2005). Arabidopsis fragile fiber8, which encodes a putative glucuronyltransferase, is essential for normal secondary wall synthesis. *Plant Cell.* **17**: 3390–3408.

Zhu, C., Ganguly, A., Baskin, T.I., McClosky, D.D., Anderson, C.T., Foster, C., Meunier, K., Okamoto, R., Berg, H., and Dixit, R. (2015). The fragile Fiber1 kinesin contributes to cortical microtubule-mediated trafficking of cell wall components. *Plant Physiol.* **167**: 780–92.

Zhu, T., Nevo, E., Sun, D., and Peng, J. (2012). Phylogenetic analyses unravel the evolutionary history of NAC proteins in plants. *Evolution.* **66**: 1833–1848.